

A support for the existence of paleolakes and paleorivers buried under Saharan sand by means of “gravitational signal” from EIGEN 6C4

Jaroslav Klokočník¹ · Jan Kostelecký^{2,3} · Václav Cílek⁴ · Aleš Bezděk¹ · Ivan Pešek⁵

Received: 12 September 2016 / Accepted: 17 March 2017
© Saudi Society for Geosciences 2017

Abstract The goal of this study is to demonstrate that and how the recent gravitational and topographic data support the findings made by geologists and others as for the existence of the paleolakes and paleoriver systems, now buried under the sands of Sahara. It is always important and useful to have such an independent analysis supporting certain results, and this paper is such a case. We make use of the gravity disturbances (or anomalies), the Marussi tensor of the second derivatives of the disturbing geopotential, the gravitational invariants and their certain ratio, the strike angle and the virtual deformations. The geopotential is represented by the global combined (from satellite and terrestrial data) high-resolution gravity field model EIGEN 6C4 (till degree and order 2160 in spherical harmonic expansion). The topography is derived from the ASTER GDEM and ETOPO 1 models (both are used). With all these data, we confirm the existence of huge paleolakes or paleoriver systems under the Saharan sands known or anticipated in an independent way by geologists for the lakes MegaChad, Fazzan and Chotts; for Tamanrasset river valley; and Kufrah Basin, presumptive previous flow of the Nile River. Moreover, we suggest a part of the Grand Egyptian

Sand Sea as another “candidate” for a paleolake and hence for a follow-up survey.

Keywords Gravitational field model EIGEN 6C4 · Functions of disturbing geopotential · Satellite digital topography models · Paleolakes/paleorivers · The Sahara · GOCE satellite

Introduction

With the best global gravitational and topographic data now available (EIGEN 6C4 and ASTER GDEM or ETOPO 1 or similar; all references below in the relevant sections), we try to support the existence of huge paleolakes and paleoriver systems under the present-day Saharan sands (Fig. 1). The lakes were discovered recently by other authors and we intend to check it completely independently of their method and/or data. This is the main goal of this paper.

The important fact is that we work not only with the traditional gravity anomalies (or disturbances) but also with components of the Marussi tensor (mainly with the second radial

✉ Jaroslav Klokočník
jklokocn@asu.cas.cz

Jan Kostelecký
kost@fsv.cvut.cz

Václav Cílek
cilek@gli.cas.cz

Aleš Bezděk
bezdek@asu.cas.cz

Ivan Pešek
pesek@fsv.cvut.cz

¹ Astronomical Institute, Czech Academy of Sciences, CZ 25 165 Ondřejov, Fričova 298, Czech Republic

² Research Institute of Geodesy, Topography and Cartography, CZ 25 066 Zdíby 98, Czech Republic

³ Geological Institute, Czech Academy of Sciences, CZ 165 00 Praha 6 – Lysolaje, Rozvojová 269, Czech Republic

⁴ Department of Geomatics, Faculty of Civil Engineering, Czech Technical University in Prague, CZ 16 629 Praha 6 – Dejvice, Thákurova 7, Czech Republic

⁵ Faculty of Geology and Mining, TU Ostrava, CZ 708 36 Ostrava, Czech Republic

Fig. 1 Relatively “topographically flat” and “gravitationally quiet” areas of the Sahara, selected for our analysis. 1 Chad (section “Lake MegaChad”), 2 Fazzan (section “Lake MegaFazzan”), 3 Chotts (section “The Chotts Megalake and to the south from it”), 4 Mauritania (section “West Sahara—Mauritania”), 5 Kufrah (section “Eastern Libya (Kufrah Basin) and northwestern Egypt (Grand Sand Sea)”), 6 Kharga (section “The Nile, Wadi Tushka and possible Kharga paleomegalake”)



derivative), the gravity invariants and their special ratio, with a non-linear combination of the components of the Marussi tensor known as the strike angle, and we add our virtual deformations. All these functions of the disturbing gravitational potential of the Earth (called also the “aspects”) are derived from the harmonic geopotential coefficients (Stokes parameters) of the recent gravitational model EIGEN 6C4. All the aspects react somehow to the density anomalies under the surface, but they have different behaviours with respect to the depth and orientation of the causative bodies (see below “Comments to theory” section and Fig. 2). The use of all the gravitational aspects enriches accessible information about the underground density anomalies (more in section “Comments to theory” section about theory).

The second section presents notes on the theory which come mostly from physical geodesy. Then, in the third section, we inform about the input data (gravitational and topographic). We comment on quality, precision and resolution of the gravitational and topographic data (see “Data” section), namely where there are some obstacles and concerns. We also warn of specific artefacts of gridding (see “Typical gravitational signal of various geological structures, note on artefacts” section and the Appendix); this is important because some artefacts can be misleading when interpreting various features or hallmarks created by the gravity field. Note for example that the resolution of EIGEN 6C4 (which is developed to degree and order 2190 in spherical harmonic expansion), projected on the Earth surface, is ~ 10 km. But in fact, the actual precision depends also on the area studied (risk of use of the so-called fill-in data). The formal commission error of the gravity anomalies (standard deviation) derived from EIGEN 6C4 is supposed to be the same or better as for EGM 2008 (~ 10 – 20 mGals over the Sahara) (see also “Data” section). It is important to note that EIGEN 6C4

(Foerste et al. 2014) contains the full set of satellite gradiometry data from the gravity mission GOCE.

The fourth section contains also few examples of typical “gravitational signal” of various geological objects. We have hundreds of such examples in our archive; we learnt with them on known geological features. Then, we extrapolated to less known or unknown features, e.g. to study highly erosive areas in Ethiopia or in the Himalayas or to seek for volcanoes under the ice of Antarctica, and here, for the paleolakes and rivers.

The fifth section is about a simple model where we show how large gravitational signal can be expected (just a rough estimate of its magnitude) from hypothetical paleolakes or rivers.

In the sixth section, we focus on particular localities, Lake MegaChad, MegaFazzan, the Chotts Megalake, West Sahara—Mauritania, East Libya (Kufrah Basin), northwestern Egypt (mainly Grand Sand Sea) and the Nile, Wadi Tushka with possible Kharga (Charga) paleolake. In all these cases,

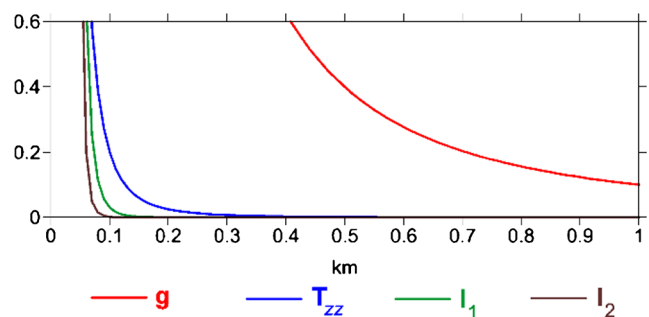


Fig. 2 Examples of decrease in the various functions of the disturbing geopotential with increasing distance (depth) from their source (the causative body represented here by a mass point, with a random value of GM). On the x axis, there are kilometres; on the y axis, there is an arbitrary quantity, dependent on GM/r^n (for a simple intercomparison of the various functions, with various powers n)

we support the independent results achieved by geologists and others. With our discrimination criterion (section “Discrimination criterion”), we can claim that our findings are well above a noise level. But one must remember that gravitational data separately, only themselves, are ambiguous for this purpose and that their interpretation will require a special care and co-action with geoscientists. We have always cooperated with other geoscientists.

Our approach is novel and it never has been used for the Sahara or similar territory by anybody else (we have recent works for other areas, see Kalvoda et al. 2013; Klokočník et al. 2013, 2016).

Comments to theory

The theory recalled and commented below comes mostly from Pedersen and Rasmussen (1990) and Beiki and Pedersen (2010) and from our recent papers (Kalvoda et al. 2013; Klokočník et al. 2013, 2016); they describe current research status in the field. The theory will not be repeated here; only a few notes follow. We recall Klokočník et al. (2016) for a review of the theory focused on our applications. But it is fair to note that the paper written by Pedersen and Rasmussen (1990) was crucial for us; in 1990, the authors worked with the second derivatives of the disturbing geopotential; their clairvoyant visions became reality with present-day existence of airborne gradiometers and with the GOCE satellite mission (Gravity field and steady-state Ocean Circulation Explorer; section “Gravitational field models with high resolution”).

The disturbing static gravitational potential T outside the Earth masses is expressed, as is usual, in the spherical harmonic expansion, in practice to some maximum degree and order. (Everywhere in this study, we work with the static not time variable potential.) The spherical approximation of the gravity anomaly or disturbance Δg is computed as a radial derivative of T . The gravity tensor Γ (the Marussi tensor) is a tensor of the second derivatives of the disturbing potential T . It contains just five linearly independent components. Under any transformation, Γ preserves three invariants I_0 , I_1 and I_2 , which are non-linear combinations of the components of Γ , where I_0 is known as the Laplace equation (it is the trace of Γ which is zero in outer space with respect to the tested body). Pedersen and Rasmussen (1990) showed that the specific ratio I of I_1 and I_2 lies always between zero and unity for any potential field. If the causative body is strictly 2D, then I equals zero.

The time when only the gravity anomalies were utilized for various geoscientific applications is already behind us. All the functions mentioned above (“aspects”) and defined in the quoted papers are derivable from a given potential T ; they have, however, different qualities and attributes, and they behave in various

ways and are sensitive in different ways to the causative body or density anomalies which produce them. We can say that they exhibit varied “gravitational signal” (while the static T remains the same). Negative gravity anomalies correspond, e.g. to thick sediment infill, while positive are linked to shallow depth basements. The second-order derivatives and the invariants provide evidence about the details of near-surface subsurface structures. They contain information about the location, size and orientation of the causative body.

The Marussi tensor was already used locally (in areas of a few square kilometres) for petroleum, metal, diamond, groundwater, etc. explorations (e.g. Saad 2006; Mataragio and Kieley 2009; Murphy and Dickinson 2009; and many others). The full Marussi tensor is a rich source of information about the density anomalies, their size and orientation, providing useful details about objects located closely to the Earth’s surface. This extra information can be used by tensor imaging techniques to enhance target anomalies, as tested for local features (economic minerals, oil and gas deposits, fault location, etc.) (see, e.g. Murphy and Dickinson 2009; Saad 2006).

The strike angle θ_S (also known as strike lineaments or strike direction) is a non-linear combination of the components of Γ . It indicates how gradiometer measurements rotate within the main directions of the underground structures. Provided that the ratio I mentioned above is small, the strike angle may indicate a dominant 2D structure. For more details, see Beiki and Pedersen (2010) or Murphy and Dickinson (2009).

The virtual deformations (vd) were introduced (defined) and used for the first time in Kalvoda et al. (2013) and Klokočník et al. (2013). The apparatus of mechanics of continuum (e.g. Brdička et al. 2000) was applied to derive the main directions of the relevant tension. It is an analogy to the tidal deformation; one can imagine directions of such a deformation due to “erosion” brought about solely by a “gravity origin”. The disturbing potential T plays a role of the potential creating a deformation. The term “virtual” is used to express that T would be able to act if rock/soil consistency (cohesion) would be zero. To illustrate vd , the semi-axes of deformation ellipse a and b are computed together in their relative size. The plotted quantities are a and b , expressed in our figures as crosses.

The computation of all quantities defined above was organized by software based on Holmes et al. (2006), later Sebera et al. (2013), using Hotine (1969), and now Bucha and Janák (2013). Many tests and intercomparisons were performed.

To be fair, we have to note that the above list of functions (aspects) of the geopotential is not complete, see, e.g. Pajot et al. (2004) or Andrews-Hanna et al. (2012) for the horizontal curvature of the potential field or its total horizontal derivative (alternatives to certain functions of the terms of the Marussi tensor).

To demonstrate how the various functions of the disturbing geopotential mentioned above behave (decrease) with

increasing distance from the source (of causative) body (a density anomaly), it is assumed that the source body is a mass point (with a selected value of GM, which is a product of the universal gravitational constant with the mass of the Earth) located on the Earth surface; all masses of the Earth are concentrated in the centre of the Earth. It is obvious that in this simplified case, some of the functions listed above do not exist or are equal to zero; the remaining functions are shown in Fig. 2. A diverse rate of decrease of the “gravitational signal” with increasing depth of the source mass body for various aspects can be seen. The slowest decrease is for the gravity anomaly (with r^2). The invariants decrease quickly (up with r^9). It tells us which aspects describe the density anomaly at the surface or in shallow depths under the surface and which are related to deeper structures (the gravity anomalies).

It may be useful to remark about another data source of remote sensing methods—the ground penetrating radar (GPR, airborne or satellite-born in our case). For the ice (e.g. Antarctica, Greenland), it penetrates kilometres through ice to bedrock or water, but for sand and rocks, it is much less—about 20 m beneath the surface of clean, dry sand, but wet sand or water is like a mirror for GPR. In this comparison, the GPR data versus the gravitational signal derived from the gravitational field models are completely independent and the latter “penetrates” much deeper under surface. However, the gravitational signal usually gives the regional large-scale picture (several to several tens of kilometre resolution), while for small/local geological and geomorphological features (metres to a kilometre), the GPR data are needed.

In our figures showing various functions of the disturbing geopotential, strongly non-linear scales are used to emphasize different kinds of geological features which otherwise might remain hidden. The gravity anomalies and/or disturbances are in milligals [mGal], the second-order potential derivatives are in Eötvös; recall that $1 \text{ mGal} = 10^{-5} \text{ ms}^{-2}$, $1E = 1 \text{ Eötvös} = 10^{-9} \text{ s}^{-2}$. The invariants I_1 and I_2 have units [s^{-4}] and [s^{-6}] and the ratio I is dimensionless. The strike angle θ is expressed in degrees with respect to the local meridian and its demonstration in red means its direction to the east and in blue to the west of the meridian. These units are used in all presented figures.

The virtual deformations (νd) are geometrically expressed by a dilatation or compression. The dilatation indicates uplifted regions at the geoid, the mass of which has a tendency to disintegrate. On the contrary, the virtual compression indicates lowered zones at the geoid. The natural processes, which are the cause of these features near the surface, are certainly very diverse as a consequence of regionally heterogeneous integration of morphotectonic, erosion-denudation, volcanic and other processes.

A systematic screening of the whole planet Earth was performed. The results of the screening were represented

by means of selected examples from regions of various planation surfaces, high mountain ranges, collision zones of oceanic and continental lithospheric plates, regional fault zones, volcanic chains and large impact craters in Kalvoda et al. (2013) and Klokočník et al. (2010, 2013) (see also www.asu.cas.cz/~jklokocn). We present some typical examples of the “gravitational signal” in the section “Typical gravitational signal of various geological structures, note on artefacts”. Then we select specific segments of the Sahara (Fig. 1) with roughly flat topography (“sand seas”) and outside mountains or trenches (with relatively “silent” gravitational signal) for a detailed inspection (“Gravitational signal and topography for selected zones of Sahara with EIGEN 6C4 and ASTER GDEM” section); the majority of them have already been recognized by geologists and others to possess large paleolakes (megalakes) or paleorivers (river systems) in recent geological history. Here, we provide an independent tool to verify such findings and maybe to do more in some cases, i.e. to suggest further places of interest for investigation by geoscientists.

Data

Gravitational field models with high resolution

The input data to our analysis are the harmonic geopotential coefficients (also known as the Stokes parameters) in the spherical harmonic expansion of the Earth’s disturbing gravitational potential; a set of these coefficients defines the gravitational (or gravity) field model. Today, global static gravitational field models of the Earth based on a variety of satellite and terrestrial data (so-called combined models) have a high resolution. The *Earth Gravitational Model 2008* (EGM 2008, Pavlis et al. 2008a, b, 2012) and *European Improved Gravity model of the Earth by New techniques* (EIGEN 6C4; Foerster et al. 2014) are both expanded to degree and order 2190 in the spherical harmonics. This corresponds to resolution 5×5 arcmin, which yields ~ 9 km half wavelength on the Earth’s surface.

In this paper, we use EIGEN 6C4. Its terrestrial gravity database is very similar (not worse) than that in EGM 2008. But more satellites were used in EIGEN 6C4 than in EGM 2008.

In many areas of Africa, terrestrial data are only “fill-in” data; it means they are computed from (satellite-born) topography data. Then, it is not surprising that the corresponding gravity anomalies and topography correlate. The areas with such data have inferior quality for our purpose. It is useful to read the paper about EGM 2008 for more details on the data quality and precision (Pavlis et al. 2012), namely pp. B04406-9, 13 or Klokočník et al. (2013, Fig. 1). For more information

about the potential danger of the fill-in data, see section “The Chotts Megalake and to the south from it” and the [Appendix](#). Fortunately, the situation is not critical for our analysis.

There is another obstacle with EIGEN 6C4 and similar gravity models: due to the data gridding before the least-squares adjustment (leading to the harmonic geopotential coefficients), the “gravitational signal” sometimes and somewhere suffers from various artefacts (more below in sections “Typical gravitational signal of various geological structures, note on artefacts” and “The Chotts Megalake and to the south from it” and in the [Appendix](#)).

With EIGEN 6C4, the medium wavelength features of the “gravitational signal” are more reliable than those from EGM 2008 for the majority of parts of the world, namely in the high mountain ranges or in remote areas like the Sahara or Antarctica; this is so due to a significant contribution of the gradiometric data (the Marussi tensor components) coming from the GOCE satellite which were incorporated into the inversion of EIGEN 6C4 (see, e.g. Foerste et al. 2014; Huang et al. 2015 and others, or www.esa.int/Our_Activities/Observing_the_Earth/GOCE).

Satellite topography data

The topography data are subsidiary for us, but they cannot be ignored. The ASTER GDEM, released in June 2009, was generated using stereo-pair images collected by the ASTER instrument (Advanced Spaceborne Thermal Emission and Reflection Radiometer) onboard *Terra* satellite (a multinational NASA scientific research satellite). The coverage of ASTER GDEM (Global Digital Elevation Model) spans from 83° north latitude to 83° south, encompassing 99% of the Earth’s landmass. We make use of the improved GDEM V2 with 260,000 additional stereo-pairs, improved coverage and reduced occurrence of artefacts in comparison with the first version of GDEM, V1. The V2 maintains the GeoTIFF format and the gridding with 30 m postings and $1 \times 1^\circ$ tiles (<https://asterweb.jpl.nasa.gov/-gdem.asp>). Pre-production estimated accuracies for this global product were 20 and 30 m at 95% confidence for the vertical and horizontal data (<http://www.gisat.cz/content/en/products/digital-elevation-model/astergdem>).

We do not use the older Space Shuttle Radar Topography Mission Digital Elevation Model (SRTM DEM, in various versions). But in few cases, we compared our plots based on the GDEM V2 with those in literature, based mostly on the Space Shuttle observations.

As an alternative source, we make use of ETOPO 1 DEM; it is a 1-arcmin (cell size) global relief model of the Earth’s surface that integrates land topography and ocean bathymetry (Amante and Eakins 2009). For the Sahara, the difference $|\text{GDEM V2} - \text{ETOPO 1}|$ is sometimes significant; then, we use Google Earth pictures to

decide which of these models might be better in a given place. In summary, we used both GDEM V2 and ETOPO 1 models.

Discrimination criterion

We were concerned about the resolution of the gravitational models (section “Gravitational field models with high resolution”). We already know that features smaller than about 10×10 km are too small to be “visible” with EIGEN 6C4.

We are also concerned about the “fill-in” data in the gravity field models (section “Gravitational field models with high resolution”). The existence of the artefacts which appear in the gravity aspects due to insufficient quality and/or resolution of the data coming to EIGEN 6C4 was also mentioned above and will be discussed more in “Typical gravitational signal of various geological structures, note on artefacts” and “The Chotts Megalake and to the south from it” sections and in the [Appendix](#).

Is there another obstacle in our analysis to provide objective results? A signal to noise ratio (S/N) should be watched too, to be sure about the statistical significance of our results, of all our conclusions. That ratio should be much larger than 3. The minimum $S/N = 3$ is our *discrimination criterion*. What is S and what is N in our case?

The S values will be derived from the actual gravity anomalies/discrepancies Δg in the area of interest according to EIGEN 6C4. The formal precision (called “commission error” in Pavlis et al. 2012, see also Fig. 2 in Klokočník et al. 2013) of the gravity anomalies for the Sahara is between 5 and 15 mGal (exceptionally ~ 20 mGal). Typically, it is 10 mGal. This is our N . It was derived by the variance-covariance transfer from the harmonic geopotential coefficients of EGM 2008 into “inaccuracy” of Δg (Pavlis et al. 2012). A similar precision estimate for T_{zz} (or other aspects of the geopotential in use here) is unknown even for EGM 2008. Similar data for EIGEN 6C4 are not available. But we know that the satellite and terrestrial database of EIGEN 6C4 is very similar or wider than that of EGM 2008 (“Gravitational field models with high resolution” section), and thus, we assume the same quality of N for both these gravity models.

It is easy to estimate, using the actual $|\Delta g|$ for all the areas studied (from the “Gravitational signal and topography for selected zones of Sahara with EIGEN 6C4 and ASTER GDEM” section) that $S/N > 3$. But this is a crude discrimination criterion. We offer here better statistics (providing even better results).

We will work with a difference of $d\Delta g$ between a typical gravity anomaly Δg_1 inside the studied area (paleolake) and anomaly Δg_2 not too far from the lake but outside of it (in the

surrounding region). The mean quadratic error $m_{d\Delta g}$ of this $d\Delta g$ is

$$m^2_{d\Delta g} = m^2_{d\Delta g1} + m^2_{d\Delta g2} - 2 m^2_{\Delta g1\Delta g2}$$

It is reasonable to assume $m_{\Delta g1} = m_{\Delta g2} \equiv m_{\Delta g}$. The quantity $m_{\Delta g1\Delta g2}$ arises from a correlation between Δg_1 and Δg_2 , i.e. $m^2_{\Delta g1\Delta g2} = r m^2_{\Delta g}$. Such a correlation must be high; if not, we would not be able (for example) to separate the geoid height variations (order of millimetres) from the geoid undulations themselves (known within decimetres, not better); we assume (from experience) the correlation coefficient $r = 0.9$. Then, we get

$$m^2_{d\Delta g} = 2 m^2_{\Delta g} - 2 \times 0.9 m^2_{\Delta g} \rightarrow m_{d\Delta g} \approx 0.5 m_{\Delta g}.$$

We take $m_{\Delta g} = N = 10$ mGal, as above. The results for the areas investigated in section “Gravitational signal and topography for selected zones of Sahara with EIGEN 6C4 and ASTER GDEM” are summarized Table 1. Always the signal to noise ratio, here $d\Delta g/m_{d\Delta g}$, is higher than 3; in other words, the improved discrimination criterion S/N says that our analysis provides statistically significant results. From the physical point of view, it means that the density anomalies beneath the surface, responsible for the relevant gravity anomalies which we “observe”, are sufficiently large in comparison with a reasonable accuracy estimate of them.

Typical gravitational signal of various geological structures, note on artefacts

The quantities mentioned above (“Comments to theory” section) were computed with the software of Dr. B. Bucha (Bucha and Janák 2013) and with our own software, and few examples are shown here to learn how the typical gravitational signal (trace, signature), generated by various geological structures, looks like.

Table 1 The signal to noise ratio of the studied areas

The area studied	Figure number ^a	Minimum S/N
Lake MegaChad	9 e	10
Lake MegaFazzan	10 c	13
Chotts Megalake	11 d	20
Tamanrasset rivers	12 a	15
Kufrah Basin	13 a	20
Wadi Tushka, Kharga		10
Grand Egyptian Sand Sea		7

^a Figure numbers that can be found under Section 6 “Gravitational signal and topography for selected zones of Sahara with EIGEN 6C4 and ASTER GDEM”

Figure 3a–c shows Mount Fuji area in Japan, the radial derivate T_{zz} of the Marussi tensor and the invariant I_2 . Fuji has a large positive value of T_{zz} . The invariants are more sensitive than T_{zz} and exhibit strong variations of the signal closely around Fuji and surrounding mountains. Then, Fig. 2c depicts vd , namely the volcanoes on the bottom of the Pacific Ocean near Japan (note positive vd inside the volcanoes surrounded by a negative value).

Figure 4a, b shows Popocatepetl and Iztaccihuatl near Mexico City in terms of T_{zz} and I_2 . It is typical that large volcanoes have the strongest gravity signal (positive values) of all mountains in their vicinity. But well visible are also “valleys” around the volcanoes (negative values of T_{zz}), which can partly be (together with stripe-like structures nearby) an artefact of gridding or of another origin. One has to be very careful to distinguish the signal coming from an actual body and from an artefact. If the causative body is small, approaching in size the resolution limit of the used expansion (here $L_{max} = 2190$ or 9 km), then a “bull-eye” effect and “stripes” may appear. The examples are in Fig. 4c, d. In Fig. 4c, we have Mt. Olymp on the planet Mars, the largest (shield) volcano in the solar system. But the current best available gravitational field model available for Mars (Marty et al. 2009) is expanded “only” to degree and order 95 (yielding a resolution of ~200 km), so even such a large object is “small” in comparison with the resolution limit, and the artefacts immediately appear (the blue zones around the volcanoes do not exist in reality).

Figure 4d shows two smaller volcanoes on the Egyptian-Libyan border, with the same artefact effect (using the resolution in spherical harmonics till 2190 of EIGEN 6C4). The “bull eye” and “stripes” are not the only types of artefacts which one can observe. In Fig. 6b, we can see the “bull eye” and “stripes” and something what we call “graining”, in T_{zz} ; these are short-periodic variations of the signal; we know that for the same area, it does not appear for Δg . We see that the higher derivative of the disturbing geopotential we have, the bigger problem with artefacts can be expected. Another form of the artefacts—a combination of “graining” with a long-periodic effect—is shown in “The Chotts Megalake and to the south from it” section and we attempt to explain it in the Appendix. These and others artefacts can be misinterpreted by a reader, so we pay some attention to them.

The large impact crater Popigai, Siberia (possibly with its smaller companions in SE-NW direction), is in Fig. 5a, b (Klokočnik et al. 2010). Note a circular “lake” inside the crater with a strong negative anomaly, surrounded by a rim with positive anomaly, even with a central peak (known well for large craters on the Moon).

The last examples are for big rivers. Figure 6a shows T_{zz} for the Great Canyon and Fig. 6b for the Amazon River.

The deep valleys are (as expected) connected with a strong negative T_{zz} . For the Canyon, the negative value is so strong (see the scale in E) that we can see it even when the width of the Canyon is shorter than the corresponding resolution of EIGEN 6C4. The Nile has also a deep (and wide) valley with conspicuous negative gravity anomaly

and the second radial derivative and with a specific orientation of the strike angle and vd (we will see in “The Nile, Wadi Tushka and possible Kharga paleomegalake” section). In a contrast, the Amazon River exhibits, however, nothing like that and it flows across a positive anomaly— Fig. 6b.

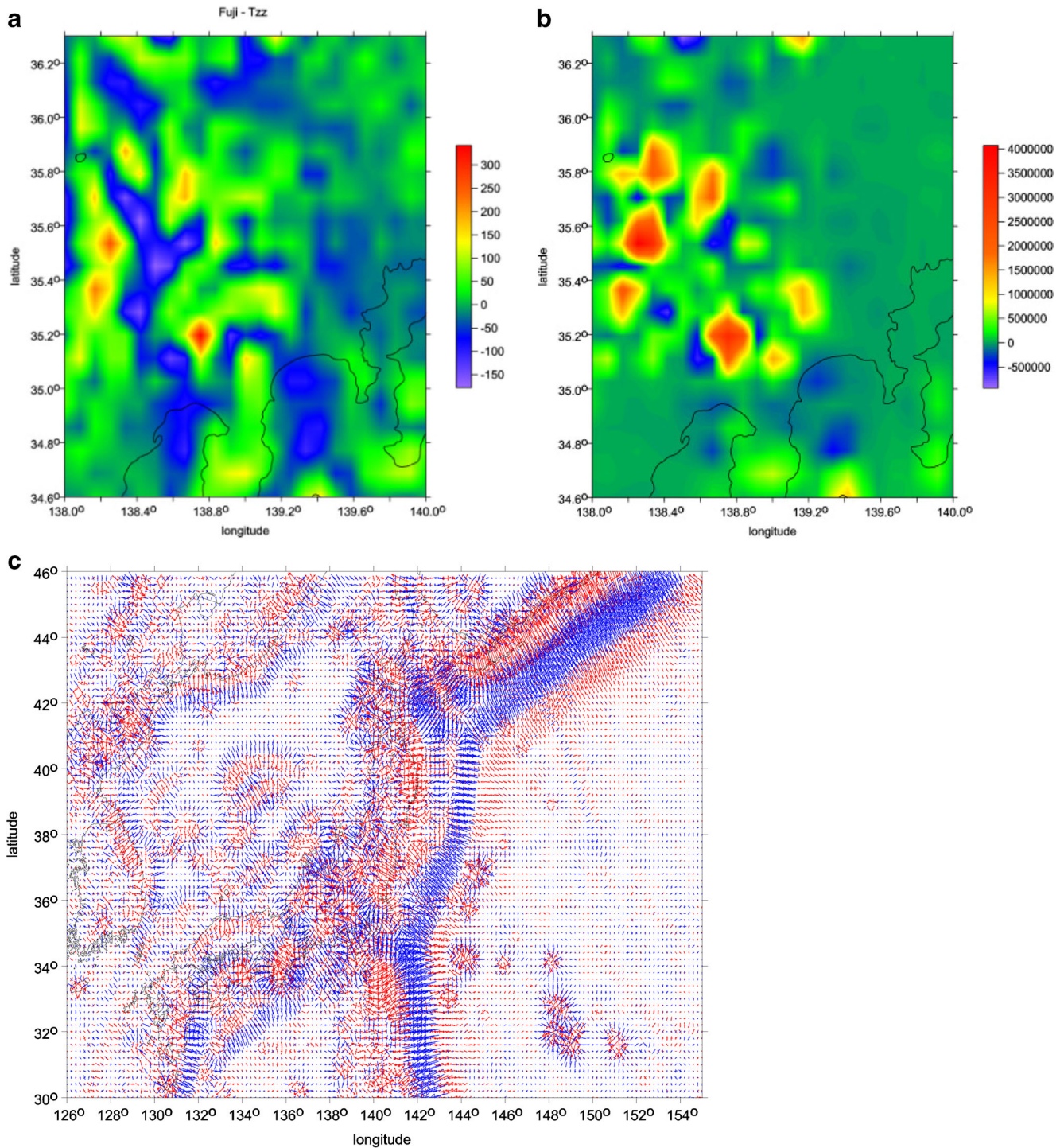


Fig. 3 a–c The radial derivative T_{zz} (a) and the invariant I_2 (b), both around Mt. Fuji in Japan, and vd , namely at the nearby trench and the volcanoes in the Pacific Ocean near Japan (c). Reproduced from Klokočník et al. (2013)

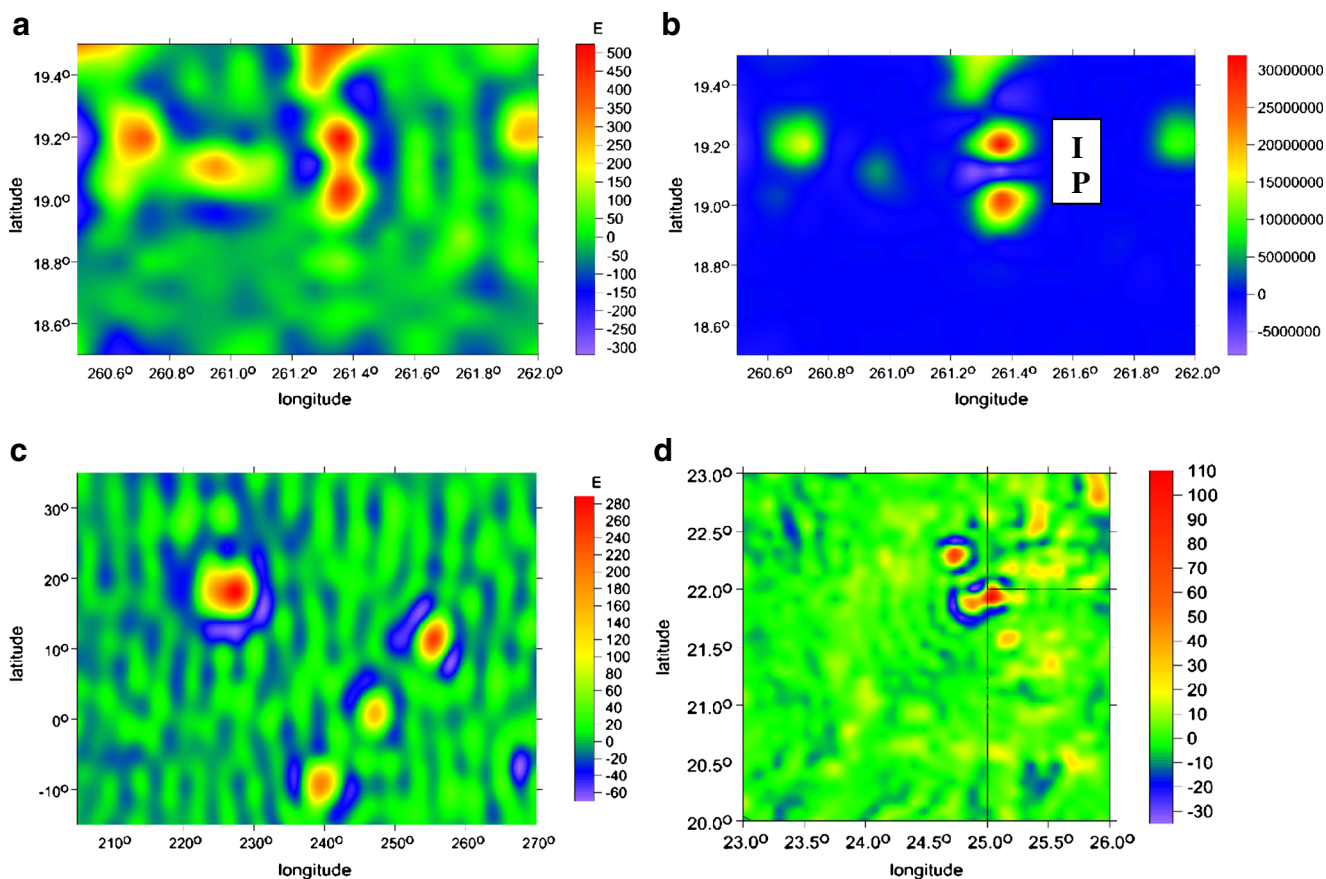


Fig. 4 a–d The largest stratovolcanoes Popocatepetl (*P*) and Iztaccihuatl (*I*) near Mexico City: **a** T_{zz} and **b** I_2 . **c** (left) The values of T_{zz} for Mt. Olymp on Mars. An example of the gridding aliasing effect (bull eye and

stripes), visible in **a** as well. **d** (right) T_{zz} for two volcanoes (Uweinat and Arkenu) on the Egyptian-Libyan border; another example of the artefacts (the bull eye and a part of rings)

Modelling the gravitational signal of a paleolake

In this section, we present a simple model of a shallow basin (paleolake) with the goal to estimate its possible gravity signal for comparison with reality (with Δg observed there now). The analysis has the following steps:

- Shape and depth of a paleolake (“the model”)
- Gravity anomaly of the model
- Comparison of the model with actual gravity signal in localities of paleolakes

To get at least a rough estimate of gravity anomalies caused by a megalake, we modelled the lake as a shallow basin in a homogeneous limestone bedrock, filled by dry sand. Two shapes of the lakes were considered, namely an elliptical lake and a C-shaped lake to approximate Lake MegaChad, with sizes 1500×300 and 1500×1100 km, respectively (Fig. 7).

In the case of large but shallow lakes, the magnitude of anomalies is practically independent of the lake shape. This happens because the mass elements at the shores are incomparably more distant from the point to be computed than the nearest elements, whose distances are limited by the lake

depth. Consequently, the closest elements dominate the magnitude of the anomaly, while the influence of the distant elements that determine the lake shape is negligible, so that the anomaly apparently depends only on the lake depth, according to the ad hoc formula

$$\Delta g = 41 \Delta \sigma h,$$

where Δg is gravity anomaly in milligals, $\Delta \sigma$ denotes relative density of sand with respect to the bedrock (in t/m^3) and h is the depth of the lake (in km). The formula is valid especially for large lakes exceeding hundreds of kilometres in diameter, which is the case of the megalakes studied here.

As a “model result”, the depth of 0.25 km yields anomalies -10 mGal that are comparable with the observed anomalies at the studied localities. Compare with the figures in the section “Gravitational signal and topography for selected zones of Sahara with EIGEN 6C4 and ASTER GDEM”, specifically with Fig. 9e for Lake MegaChad, Fig. 10e for Fazzan, Fig. 12e for West Sahara River system and Fig. 13e for East Libya and the Kufrah River system. The extensive area south of the Chotts, Fig. 11d, is not explained by the presence of lake only; h should be much higher.

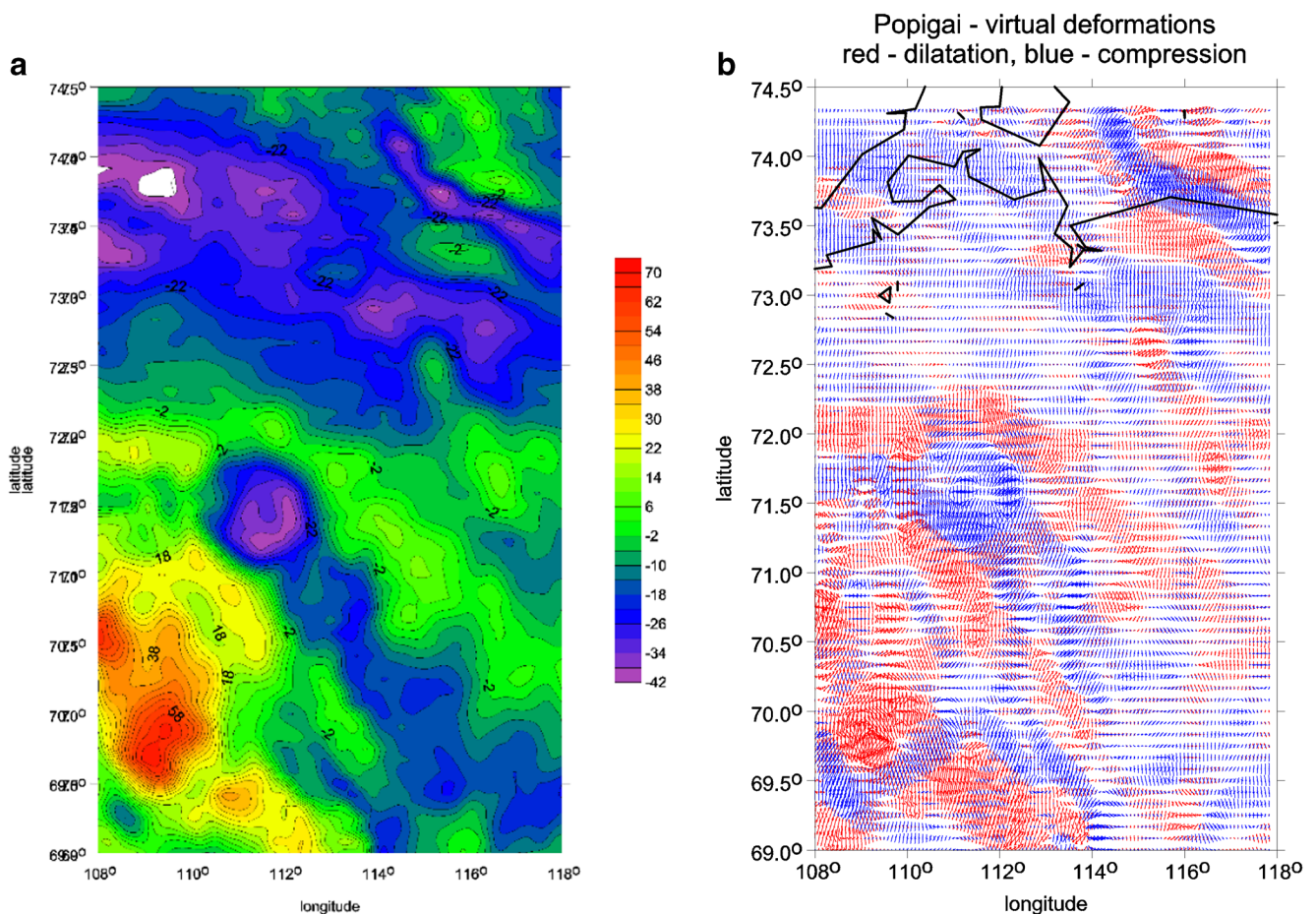


Fig. 5 a Δg and b vd for the large impact crater Popigai, Siberia (diameter of the main crater on the west side of our figure is about 100 km). More in Klokočník et al. (2010); possibly a multiple crater

Gravitational signal and topography for selected zones of Sahara with EIGEN 6C4 and ASTER GDEM

Introductory note

The functions recalled in the section “Comments to theory” were computed and plotted for the whole planet Earth, in step $5' \times 5'$ with EIGEN 6C4 and with ASTER GDEM V2 or ETOPO 1 in the same step. Many examples of the “gravity maps” were already presented [e.g. Kalvoda et al. (2013), Klokočník et al. (2010, 2013)]. Here we focus on the individual segments of the Sahara, where geologists and others found lakes and rivers now mostly or completely parched and covered by sand. We will show whether and how the gravitational signal may contribute to a confirmation and perhaps also to an extension of their discoveries.

We recall that from the gravitational signal alone, one cannot infer on the causative body in a unique, unambiguous way; one and the same signal may be generated by various density anomalies. We are aware that the gravitational signal is most sensitive to recent geological structures or structures not yet modified by various geological processes which have appeared meantime. We also recall Fig. 2 where we showed the behaviour of various

functions of the disturbing potential (the gravitational signal) for increasing depth of the causative body; it indicates that while the gravity anomalies are sensitive more to the density anomalies located deeper under the surface, the invariants react dominantly on shallowly deposited bodies or their parts. The strike angle and the virtual deformations provide a specific directional and dynamical information, although we always (everywhere in this study) use the *static* gravitational field models (only the EIGEN 6C4 in our case).

Our choice of the areas in the Sahara (Fig. 1) is focused on the places relatively “gravitationally silent”, calm and being undisturbed by mountain belts, fracture zones, etc. All selected segments have nearly flat topography (“sand and dune seas”) but not “flat” gravitational signals. We know about fill-in data in EIGEN 6C4 in some areas of the world and we hope that it is not often the case in the areas studied here (section “Gravitational field models with high resolution”, although Fig. 1 in Klokočník et al. (2013) is a warning, but information about the terrestrial data in EGM 2008, and in turn also in EIGEN 6C4, are not complete). We are aware of the fact that the quality of that terrestrial part of the data used in EIGEN 6C4 for the Sahara is not the best.

Let us note also that our gravitational signal is independent of the data from the quoted literature. Also the digital models

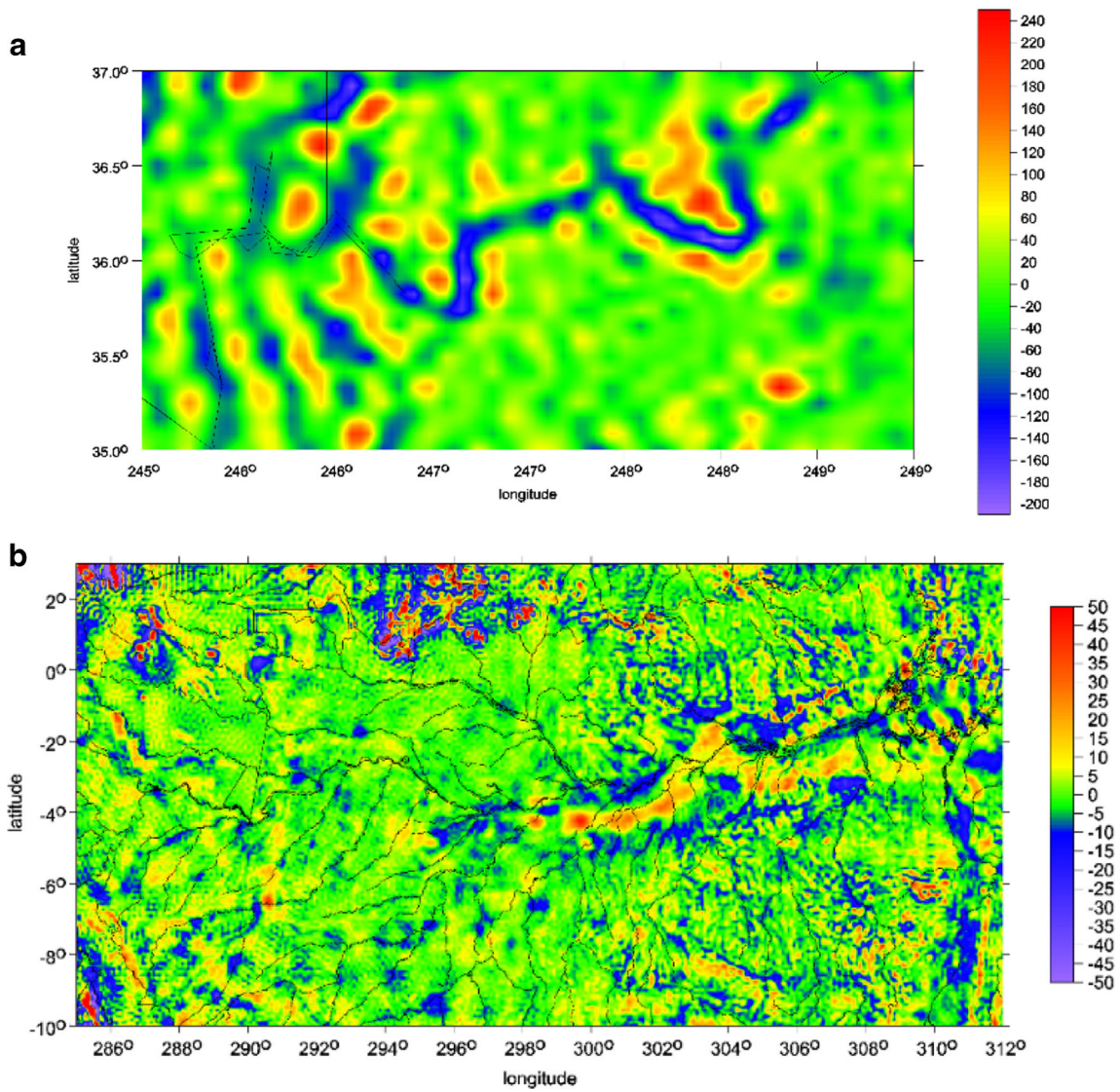


Fig. 6 a, b The values of T_{zz} in the Great Canyon (a) and across the Amazon River (b)

Fig. 7 A model of the paleolake of C-shape as a shallow basin in a homogeneous limestone bedrock filled by dry and clean sand. The basin is limited from SW-NE side by a fault system. Scale in [mGal]. See also “Lake MegaChad” section

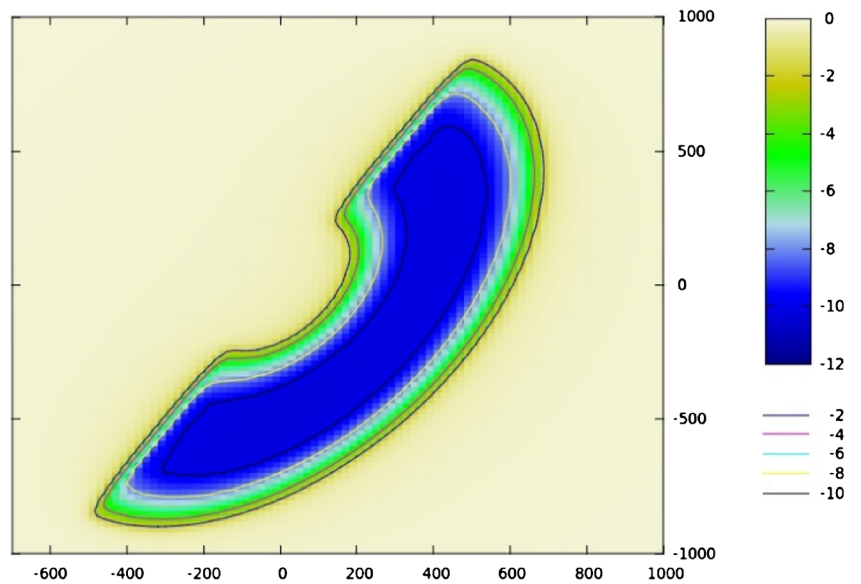
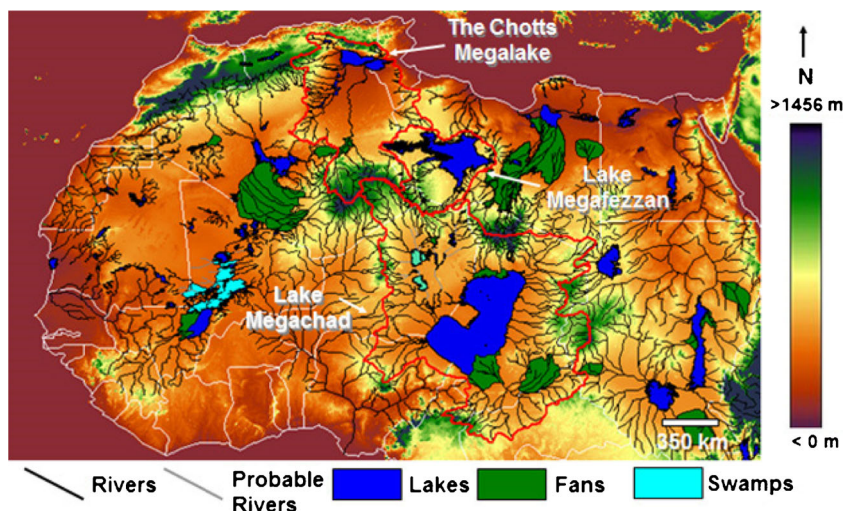


Fig. 8 Lakes and rivers under the sands of the Sahara. It was a “paradise” few thousand years ago, with verdant fields, lush country, a vast river system, swamps, lakes and a few inland megalakes



ASTER GDEM and ETOPO 1 come from other sources than the data in those papers (their source is often, at least partly, the Space Shuttle Radar Topography Mission Digital Elevation Model).

A sketch of the lakes and rivers already discovered, buried under Saharan sand, is in Fig. 8 and is reproduced from Internet materials of the Sahara Megalakes Project (King’s College London). We test these localities (megalakes on the Sahara), and more, in the following sections. For more about the geology of Africa, see, e.g. Schlütter (2006).

Note also a long-term discussion on the timing of orbital-scale monsoon changes (see namely Kuper and Kröepelin 2006); the hypothesis applies the well-known Milankovitch theory and tries to explain the North African climate cycles (“green” versus “desert” Sahara).

Lake MegaChad

The Lake Chad (also called Small Lake) now sits on the borders of Chad, Nigeria, Cameroon and Niger (Fig. 9a, b). It is still reducing its size significantly (the reader can compare “historical images” on Google Earth). In the past, it was much bigger (Fig. 9c), and it was the second largest inland lake in the world after the present-day Caspian Sea. Armitage et al. (2015) reconstructed the lake-level history; they claim that the humid period ended abruptly 5000 BP [BP = before present]. The oldest archaeological sites found near the former shores of the Lake MegaChad are 4000 years old, already from the time of desiccation, and are at an altitude of ~300 m (metres above today’s mean sea level). The contour line 325 m (when the megalake should be the largest in its recent geological history,

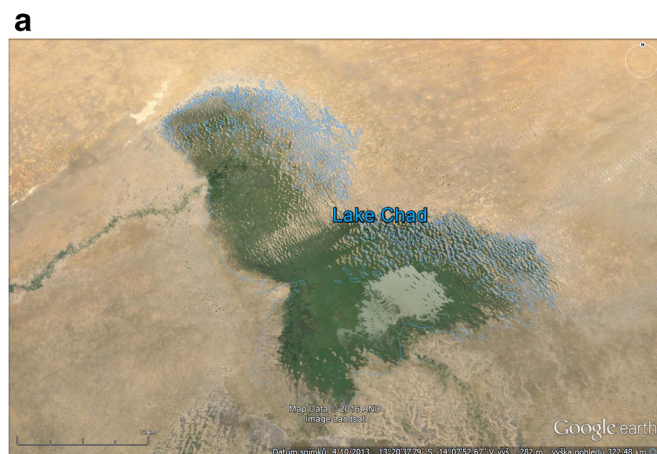


Fig. 9 a, b The Lake Chad and its surrounding area today (© Google Earth). Centre of **a** has latitude and longitude $\varphi = 13^\circ \text{ N}$ and $\lambda = 14^\circ \text{ E}$. **c, d** The Lake MegaChad (reproduced from Leblanc et al. 2006, their Fig. 1) and topography according to the ASTER GDEM V2. The contour line with 325 m is marked. The gravity data suggests a continuation of the paleolake in the N-NW direction from the present-day remnant of the lake or the existence of a sedimentary basin with two deeper centres that may

indicate at certain point of desiccation two independent lakes with larger and more important now completely dry area NW of the present lake. **e–i** The gravity disturbances Δg (**e**); the second radial derivative, a component of the Marussi tensor T_{zz} (**f**); one of the gravity invariants I_2 (**g**), the strike angle θ (**h**), and the virtual deformations (blue for compression, red for dilatation) vd , (**i**) with EIGEN 6C4 (till degree and order 2190) in step $5' \times 5'$ (~9 km)

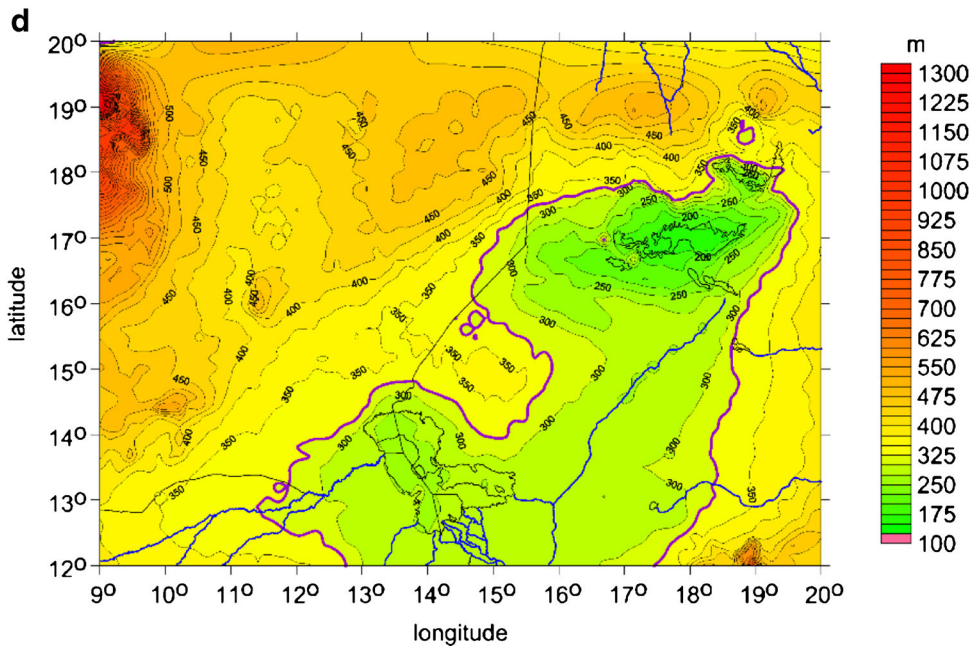
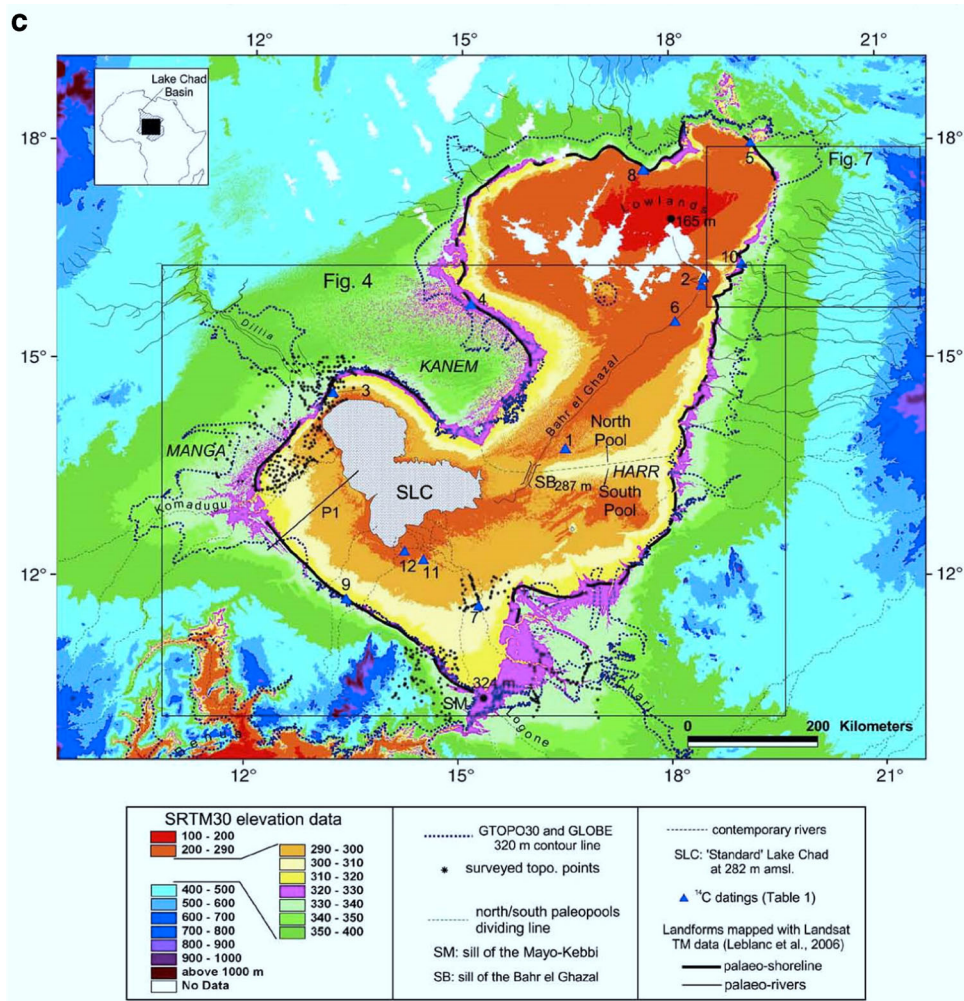


Fig. 9 continued.

15,000–11,500 BP) is shown in Fig. 9c (from Leblanc et al. 2006). See also Schuster et al. (2005). This contour line is marked also in the topography map from the ASTER GDEM in Fig. 9d.

We compare our results also with Lopez et al. (2016), namely with their Fig. 2 showing gravity anomalies and locations of piezometric domes and depressions (see below).

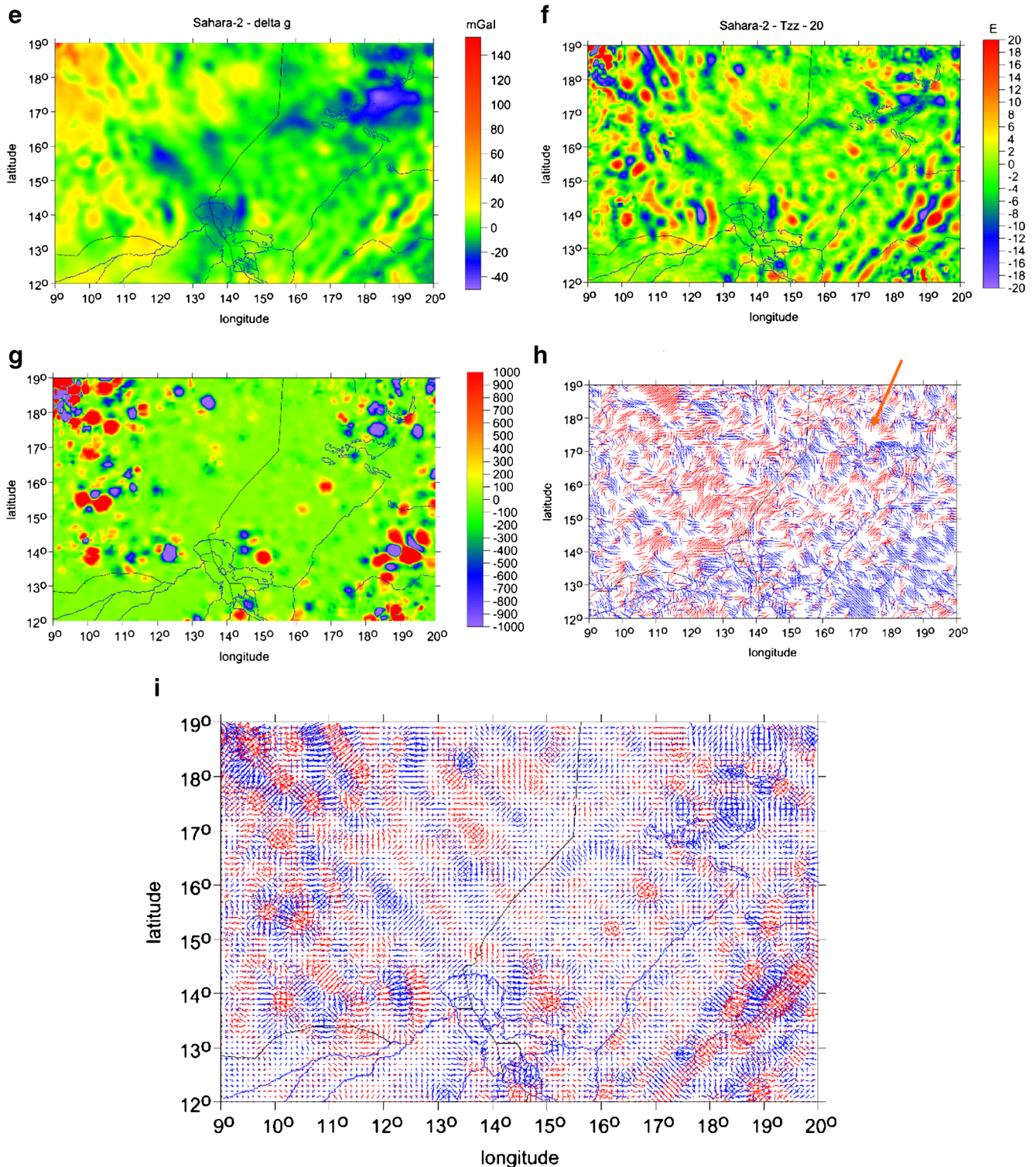


Fig. 9 continued.

There is a debate about a possible path for the Megalake Chad to discharge into the Mediterranean Sea via the Kufrah Basin in east Libya (see “Eastern Libya (Kufrah Basin) and northwestern Egypt (Grand Sand Sea)” section) or to the southern Niger (Drake et al. 2008). Taking into account our gravitational and topographic data (Figs. 9e–i and 13c–f), such a “connection” was feasible.

Our results are presented in Fig. 9d (the topography) and e–i (for the gravitational signal with EIGEN 6C4 model). The northern part of the megalake (including the Bodélé Depression) reveals very well negative disturbances Δg and second radial derivatives T_{zz} (Fig. 9e, f). Present-day

remnants of the megalake on the NW side have also negative Δg and T_{zz} . All these correlate well with the compression of the virtual deformations vd . The “negative” structures in N and NE (see arrow in Fig. 9h) have probably a deeper density anomaly origin—the structures are noticeable in Fig. 9e–i but not in Fig. 9h; there one should not expect a flat causative body. The paleolake may continue in the NW direction from the present position of that remaining lake.

Our results support the existence of the Lake MegaChad, and at a certain point of desiccation, they may indicate two independent lakes with larger and more

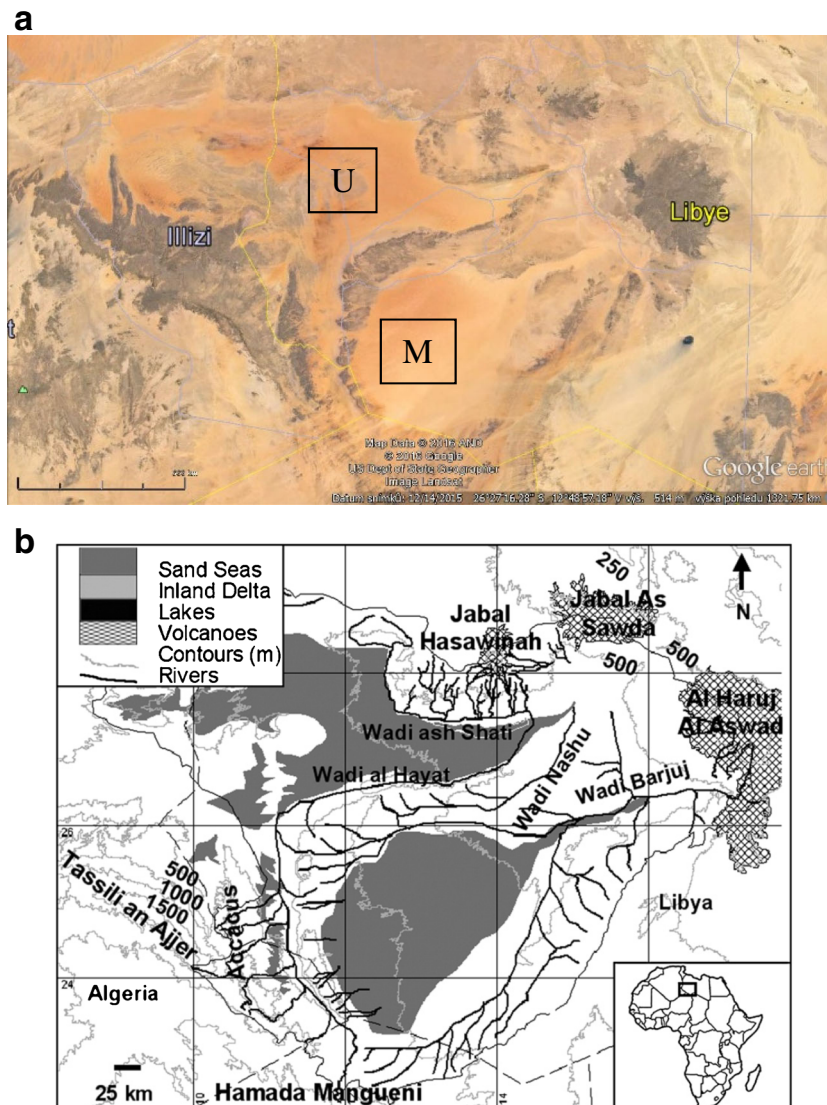


Fig. 10 a, b The Fazzan Basin and surrounding area according to © Google Earth; centre of a has $\varphi = 26^\circ \text{ N}$ and $\lambda = 13^\circ \text{ E}$. There are two big sand seas in the Fazzan (M Murzuq and U Ubari). The Fazzan Basin topography derived from STRM DEM with the main river channels, sand seas and volcanoes is marked. The catchment boundary of Lake

MegaFazzan is shown as a *thin black line* (reproduced from Drake et al. 2008). More detailed topography is given below (h). c–h The Fazzan Basin and surrounding area with Δg (c), T_{zz} (d), I_2 (e), θ (f), vd (g) with EIGEN 6C4 and the topography from ASTER (h). The symbol H means Wadi al Hayat and Wadi Nashu with a belt and a cliff between them

important now completely dry area NW of the present lake. This agrees with the piezometric map in Fig. 4 in Lopez et al. (2016).

A comparison of our results with (Lopez et al. 2016, their Figs. 2 and 4), namely using our Fig. 9e–g, i, shows a fair agreement of geographic positions of non-distinct negative

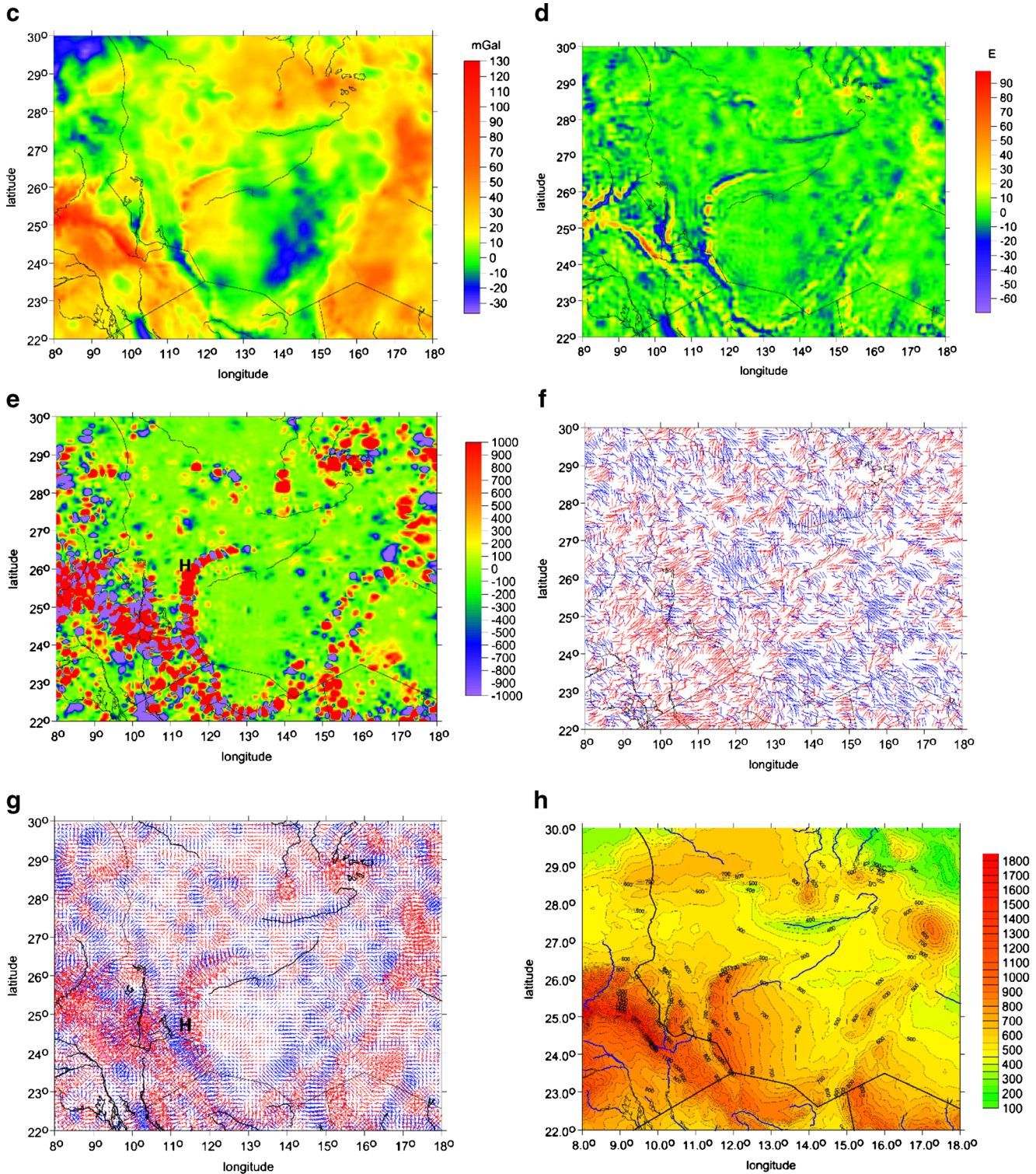


Fig. 10 continued.

gravity anomalies, negative second derivatives, extremes of the invariants and the virtual deformations with the positions of piezometric depressions. But the gravity signal is influenced by a variety of density anomalies coming from diverse sources, such as volcanic bodies, and thus, a relation between the gravity signal and the domes/depressions is not unambiguous.

Note that we also confirm the Chad lineaments found by Braitenberg et al. (2011)—who worked with EGM 2008 at that time. Namely, Fig. 9f, i shows various interesting details and Fig. 9g shows the extrema of I_2 (compare to Fig. 4a, b in the Braitenberg et al. study), leaving this for further investigation by specialists.

Lake MegaFazzan

The Lake Fazzan (Fezzán) was in what is now west Libya (and a small part was in Algeria) (Fig. 10a). Drake et al. (2008) used information on topography, geology and

geomorphology to develop a chronology for the development of Lake MegaFazzan. A giant lake has existed periodically in the Fazzan Basin since the late Miocene (7–5 million years ago). The largest possible extent of the lake (~3 million years ago) is shown in Fig. 13 in Drake et al. (2008); we use here their Fig. 2 and reproduce it as Fig. 10b. Later lake phases were smaller, and the interglacials less humid. The last humid phase started about 10,000 BP but was interrupted by abrupt intensification of aridity.

EIGEN 6C4 shows the Fazzan Basin in terms of the gravity disturbances Δg and the radial component of the Marussi tensor T_{zz} (Fig. 10c, d). The place for possible megalake is clearly marked. Figure 9c, d correlates very well with Fig. 10a, b. The gravitational signal cannot geolocate exactly the paleolake but can confirm or at least support independent geological findings (e.g. Drake et al. 2008, the Sahara Megalakes Project) about the existence of such megalake. The invariants disclosing shallowly deposited density anomalies delineate the shape of

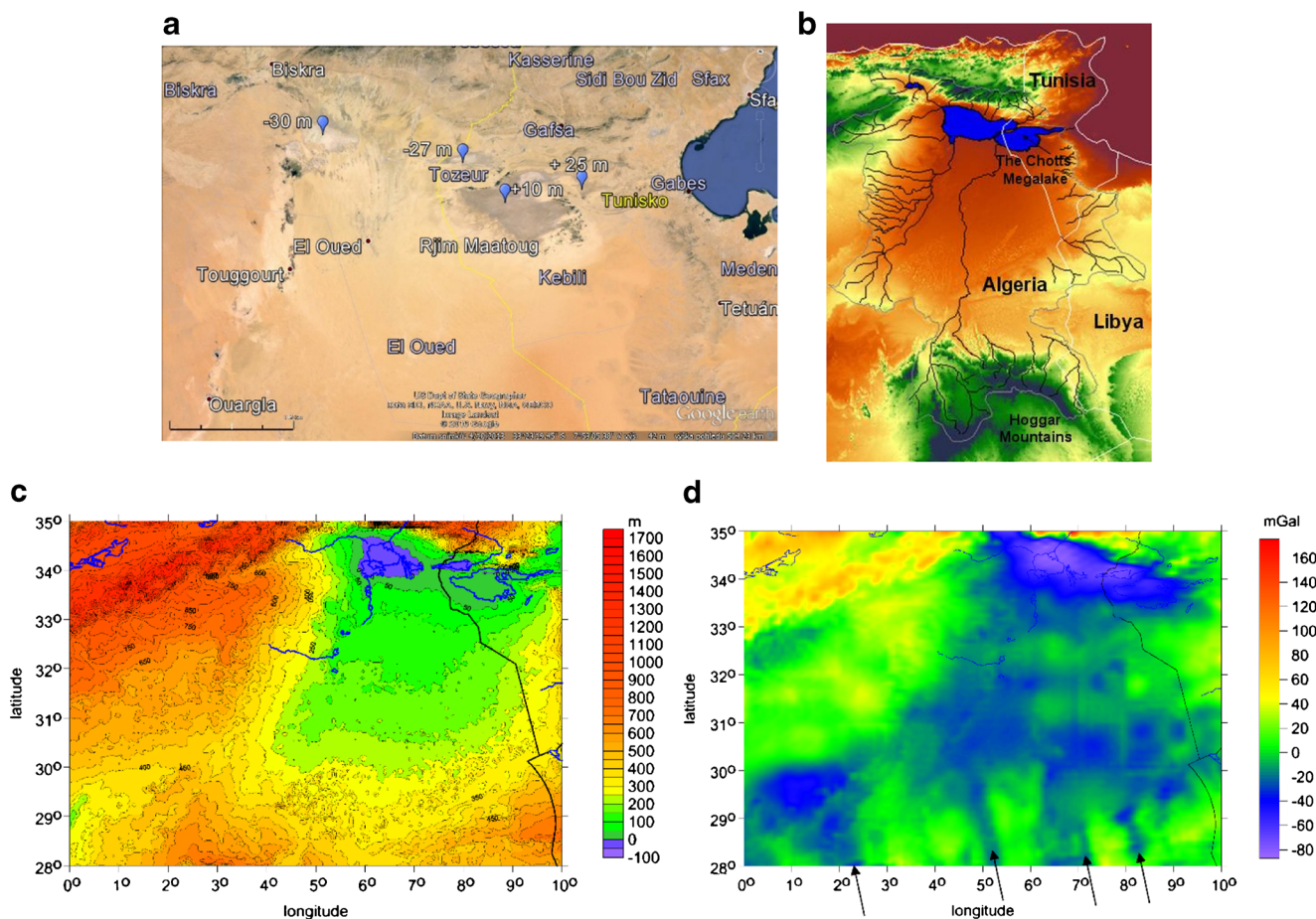


Fig. 11 **a, b** Left **(a)** The area of the Chotts Megalake (including Chotts Melhir, El Gharsa, El Jerid and El Fejej depressions, from west to east) according to © Google Earth; Tezeur oasis in **a** has $\varphi = 34^\circ \text{N}$ and $\lambda = 8^\circ \text{E}$. **b** Shuttle's DEM of the Chotts Basin (Kings' Coll.) with the catchment area and the main rivers and lakes overlaid. **c–g** ASTER GDEM topography **(c)** and **d–f** the gravitational signal with EIGEN 6C4

model. Note the extensive and deep negative Δg **(d)** and T_{zz} **(e)** and anomalous I_2 **(f)** in the area where the megalake is supposed, but more rivers/aquifers and lakes might be hidden under sand in S and SW directions from the megalake **(e, g)**. Peculiar artefacts (circled) are discussed in the text. *Blue colour* in **c** does not mean water but that the terrain is below sea level

the basin (see I_2 in Fig. 10e and the symbol H for Wadi Hayat); compare with sharp geomorphology around H in Drake et al. (2008). On possible coast of the paleolake, the strike angles θ have a tendency to the same orientation (blue vectors in Fig. 10f, oriented mostly NS or NW/NE). The zones of compression of νd in Fig. 10g follow the rivers (east and west of the circular-like belt) and concentrate in the eastern and northern parts of the basin (where we expect the deepest part of the megalake). The belt between Wadi al Hayat (Hayaa) and Wadi Nashu is shown as a dilatation (Fig. 10c, d, and positive extremes of I_2 in Fig. 10e), a possible shore of the southern part of the paleolake on its eastern side also. With the gravitational data we presented in this section, we can imagine Lake MegaFazzan roughly as was “located” by geologists (see Fig. 10b), with possible continuation to NW from the poor present-day rest of the lake. Topography from ASTER is shown in Fig. 10h. Our results support the existence of Lake MegaFazzan.

The Chotts Megalake and to the south from it

The Chotts Megalake (now salt pans-sabkhas and a series of low-altitude saline seasonal lakes, marshland and basins in a depression in Tunisia and Algeria) was fed by several rivers from the Atlas Mountains and two large river systems flowing from the south from the central Sahara (see, e.g. Internet materials of the Sahara Megalakes Project, King’s College London). For geology evolution of this and surrounding areas, see Patriat et al. (2003).

Several mythological sources point to there being a large lake where the Chotts el Jerid and other chotts currently reside. In particular, this region has been regarded as the location of “Lake Tritonis”. Is there any evidence that this body of water emptied during the Bronze age or earlier? The answer is yes (see Battarbee et al. 2004; Kafri and Yechieli 2010; Hoelzmann et al. 2004, etc.).

With Google Earth and with ASTER GDEM (Fig. 11a, c) we can imagine the location of the megalake and how it

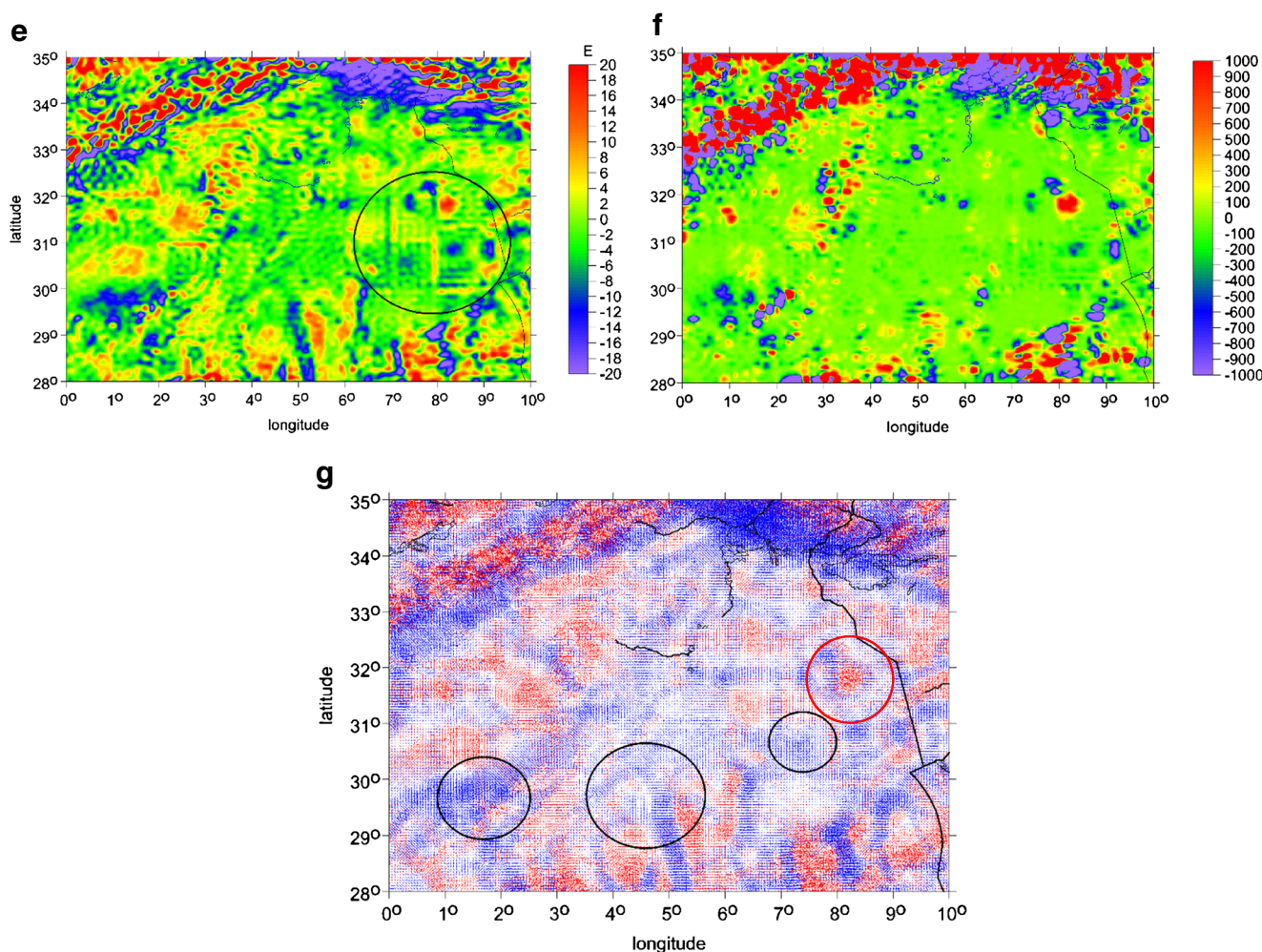


Fig. 11 continued.

overcame today’s height difference ~40 m north of towns Fatnassa and Al-Hammah to enter the Mediterranean Sea in the east direction (Fig. 11b). This agrees well with Kafri and Yechieli (2010) about hydrology systems of this area.

Our results are presented in Fig. 11c (the topography) and d–f (for the gravitational signal with EIGEN 6C4 model). Obviously, both topography and gravity support the existence of the megalake, but more so, they insinuate that the negative Δg (d) and T_{zz} (e) or anomalous I_2 (f) of a large extent may be a sign of possible paleolakes or swamps and rivers also in the S and SW directions from the Chotts Megalake location, known as Grand Erg (Sand Sea) Oriental. Note that only a part of this area is represented by the fill-in data in EIGEN 6C4; they have better data here. Our results support the existence of Lake MegaChotts; moreover, for the first time, we are not in a role just to confirm or support features known to geologists, but we suggest further research, namely in the south directions from the Chotts, where we can expect three to four river tributaries (see arrows in Fig. 11d).

We are familiar with various types of artefacts (see Fig. 4a–d). Figure 11d–e, g exhibits very peculiar “objects”, like very long walls. These are huge rectangular structures with side of more than 100 km long, together with small size “graining”. It hardly can be a real (man-made?) object. Also, note circular structures in that area, usually with negative Δg and T_{zz} , with one stronger positive value at ($\varphi = 32^\circ$, $\lambda = 8.5^\circ$ E, see the red circles in Fig. 11e, g). Recall that sand surface in that area is generally flat (confirmed by Fig. 11a, c). We did not observe such lineaments elsewhere; it is strange that they appear solely in this area where better gravity data than is usual for the Saharan territory are available with EIGEN 6C4 (see Fig. 1 in Klokočník et al. 2013; these should be the NGA LSC data, see Pavlis et al. 2012). Both structures remain enigmatic features possibly caused in case of rectangular grid probably by an interaction of the actual tectonic structures with the computational artefacts. We try to explain their origin (see Appendix).

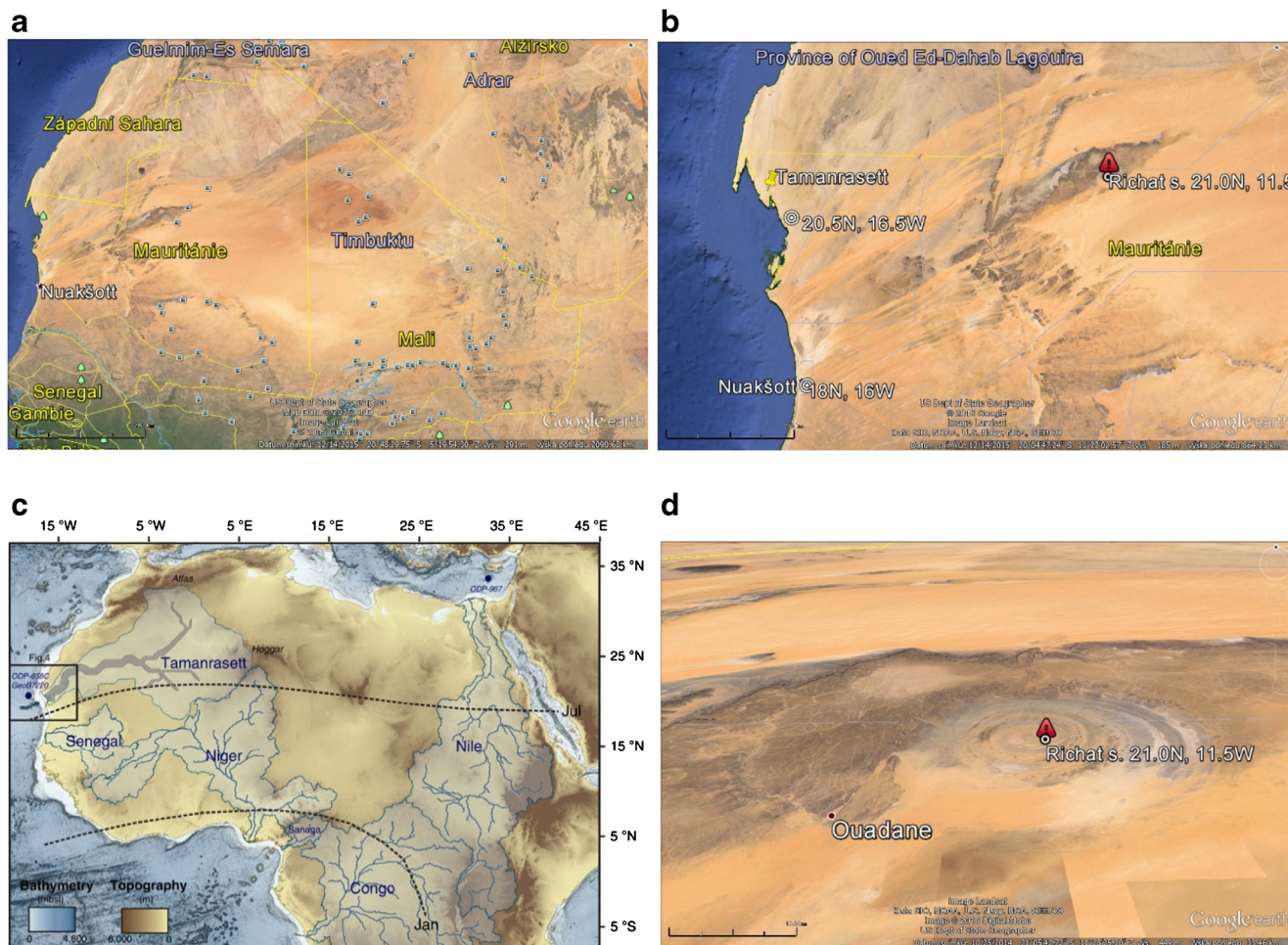


Fig. 12 a–h Mauritania, West Sahara: **a** © Google Earth general, **b** zoom for the western part to the Atlantic Ocean, **c** map of possible Tamanrasett river valley (reproduced from Skonieczny et al. 2015), **d** zoom of Google

Earth for the Richat structure near Ouadane, **e** Δg and **f** T_{zz} of catchment(s), **g** vd and **h** topography from the ASTER GDEM (the Atlantic Sea is without any data), from El Djouf Sand Sea to the ocean

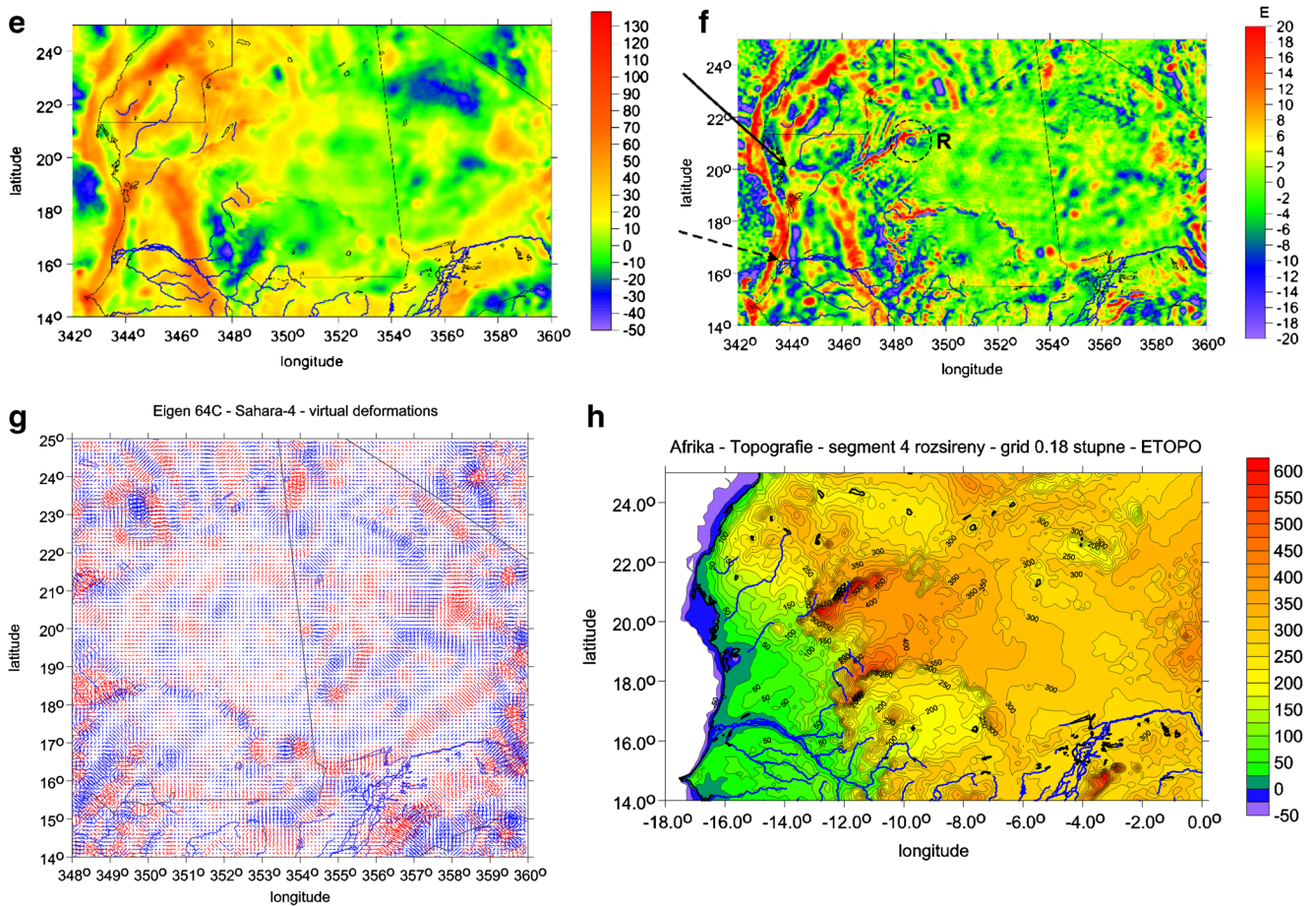


Fig. 12 continued.

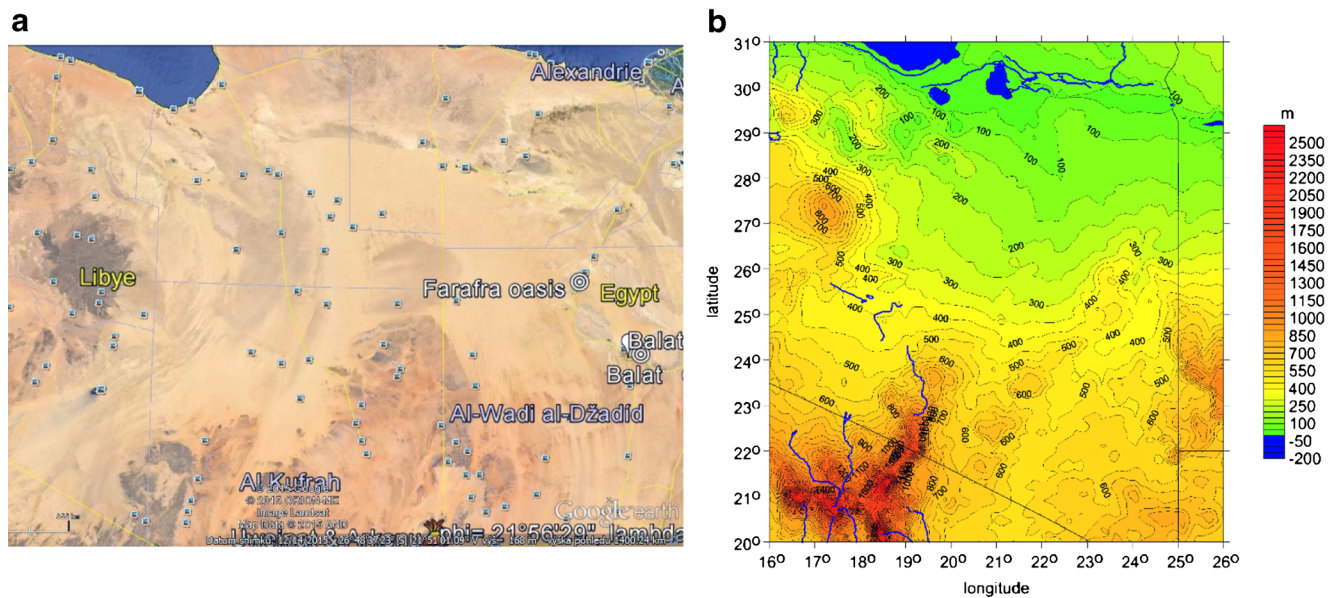


Fig. 13 a–f East of Libya and the Kufrah River system. **a** Topography according to © Google Earth, **b** topography according to ASTER GDEM V2, **c** Δg with EIGEN 6C4, **d** T_{zz} with EIGEN 6C4 and **e** the Kufrah River paleodrainage system and the Wadi Sahabi paleochannel (in blue) mapped onto a Landsat mosaic. The hypothetical two paths according to Paillou et al. (2012) and older literature (for references, see Paillou et al.

2012). **f** vd with EIGEN 6C4 (note different scales in overlapping **f** and Fig. 14b) to emphasize what we need to display). **c** Contains our suggestion for a possible paleoriver—see the dashed line overlying the gravity disturbances. **d**, **f** Indicate that there are more candidates for possible flows of paleoriver(s). See also Fig. 14a–b, f. Compare to Fig. 13e, coming from an independent study (Paillou et al. 2012)

West Sahara—Mauritania

Large generally flat sandy areas are in Timbuktu, Mali and Mauritania, with a modest slope to the W from altitude 300 m (and more) to the Atlantic Ocean. Figure 12a, b shows these areas by © Google Earth. Hypothetical paleoriver

network underneath West Sahara sands was discovered in this area with radar imagery (Skonieczny et al. 2015) as part of the enormous Tamanrasset river valley (Fig. 12e), comparable with present-day Ganges-Brahmaputra river basin in Asia.

We agree with such findings, judging from Fig. 12e–g, and we support them and can extend them. We would agree with

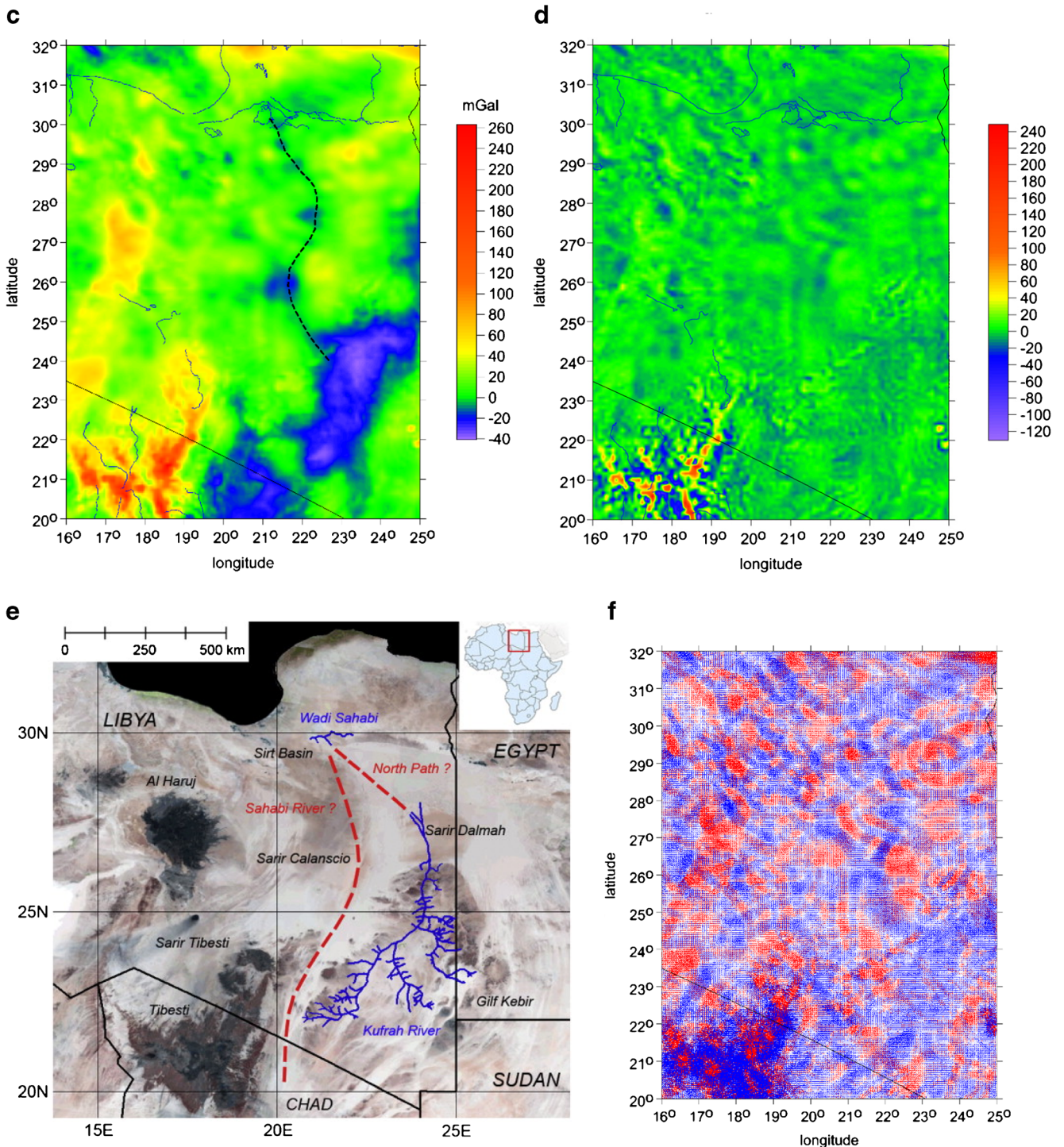


Fig. 13 continued.

two and may be four estuaries—see Fig. 12h, all this in accord with Fig. 12f. Note, however, that this area suffers from the fill-in data use in the gravity field models (Pavlis et al. 2012).

The circular feature at $\varphi = 21.0^\circ$ N and $\lambda = 11.5^\circ$ W (Fig. 12b, d) near Ouadane town, visible perfectly also in T_{zz} (Fig. 12f), is the Richat structure (the Eye of the Sahara) with a

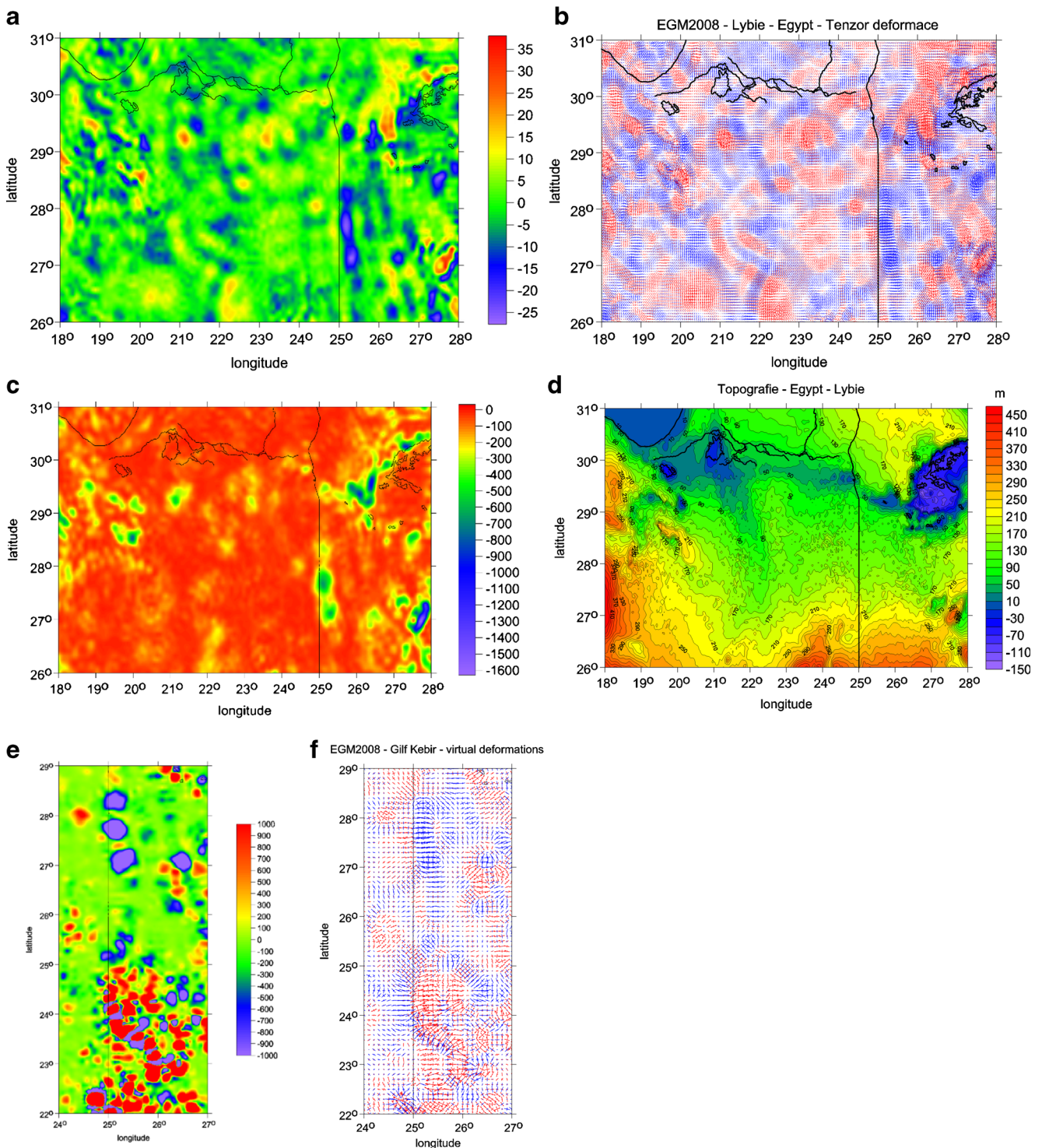
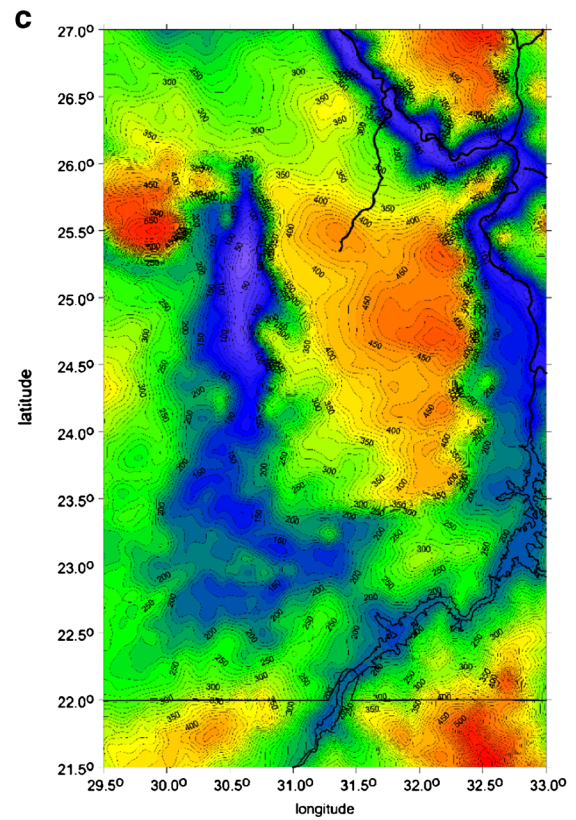
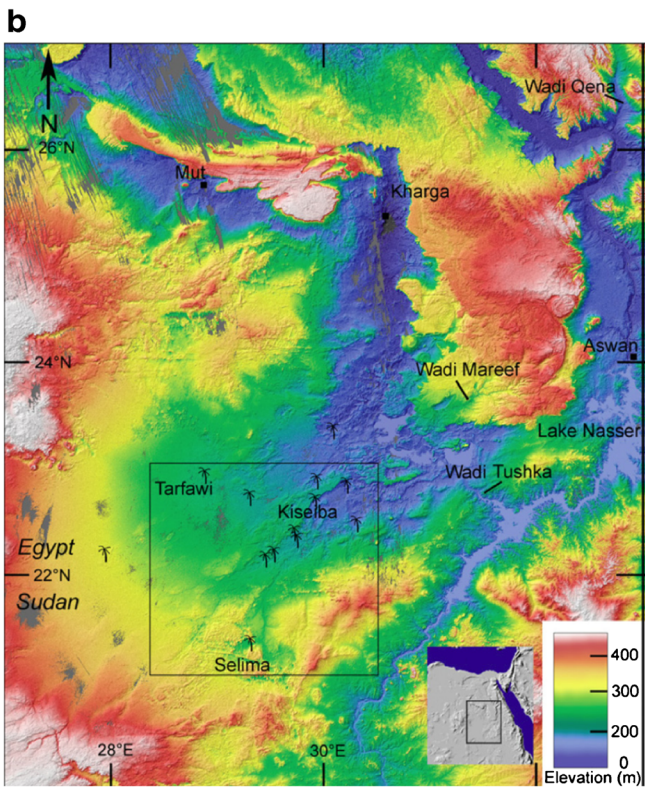
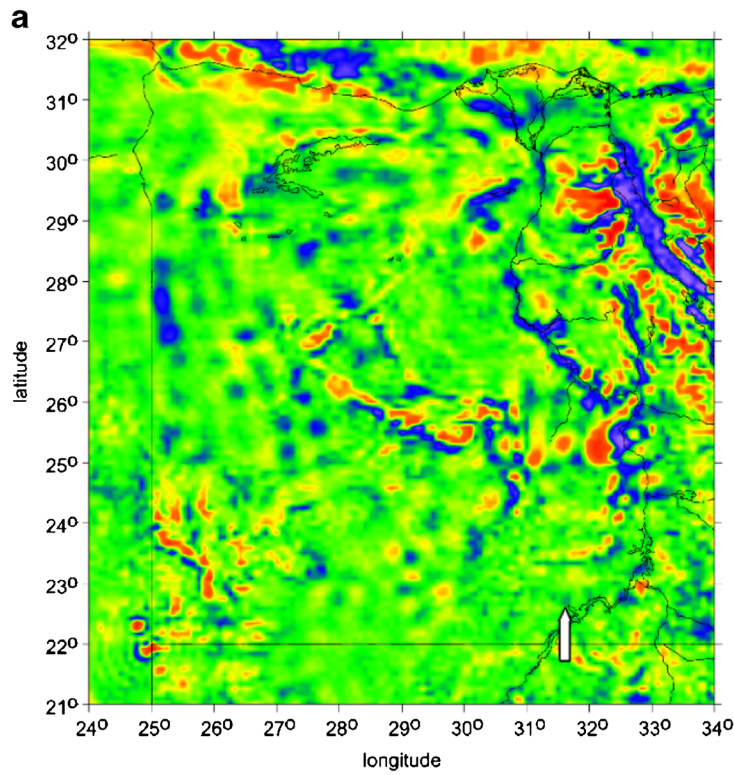


Fig. 14 a–d Grand Sand Sea in West Egypt and a part of eastern Libya: a T_{zz} , b vd, c I_1 and d topography from ASTER GDEM. To the suggested paleolake and indication of large river flow from south to north to Siwa depression and/or to the western coast of Libya. Note less visible NS

structure in eastern Libya that may represent the relicts of another large river. e, f A possible lake(s) and a flow of a hypothetical paleoriver to the area of the Grand Sand Sea in West Egypt north of Uweinat and Arkenu, south of Siwa: e for I_2 , f for vd



◀ **Fig. 15 a–c** More chances for paleolakes and paleorivers in the Sahara. **a** Strong negative T_{zz} of the Nile River valley, Faiyum oasis, delta of the Nile, Grand Sand Sea, Western Desert, Siwa/Qatara depressions, Wadi and lakes Toshka (white arrow), connected via relicts of lakes to the area of Baris and Kharga (with possible paleomegalake); **b, c** topography of the Kharga and Wadi Toshka area from two independent sources; see next captions. **b (left)** Topography of southern Egypt and adjacent Sudan from SRTM DEM. Middle Pleistocene (approx. 0.5 Ma) overflow of the Nile River to the west through the Wadi Toshka was proposed to account for lake remnants, fossil fish and paleochannel terminations at a level 247 m (see Maxwell et al. 2010). Compare to the topography from ASTER GDEM (in **c**). **c (right)** ASTER GDEM of the same area as in **b** (but independent source). Water flowed through Wadi Toshka into a megalake (Maxwell et al. 2010) reaching on its northern side Kharga. Compare to the SRTM DEM (in **b**). **d** Detail of terrain near Wadi and Lakes Toshka, **e** zoom of T_{zz} and **f** vd with possible flow of the past Nile from Wadi Toshka in west direction to East Oweinat, then to north to the Kharga area

diameter about 40 km. It was initially interpreted as a meteoritic crater (even coesite was found there, but later it was recognized as a misidentification, Dietz et al. 1969), so now geologists think that it is an eroded geologic dome (e.g. Jesus et al. 2011; Matton and Jébrak 2014). The gravitational signal itself would not exclude its impact origin, but the outer ring on its southern side would be already disintegrated by some process (compare Fig. 12d, f to Fig. 5a, b). Our results support the existence of the paleoriver network in West Sahara.

Eastern Libya (Kufrah Basin) and northwestern Egypt (Grand Sand Sea)

Here we deal with the area of eastern Libya and Grand (Egyptian) Sand Sea in NW Egypt. For the geology of this area see, e.g. Salem and Busrewil (1980). We show the topography of those areas via © Google Earth in Fig. 13a, via ASTER GDEM in Figs. 13b and 14d and the gravitational signal in Fig. 13c–f. Drake et al. (2008) or Paillou et al. (2012), among others, studied the Kufra(h) paleodrainage system, and processing of the US SRTM topographic data and Japanese PALSAR radar images suggested a path of the river system to N to the Mediterranean Sea (Fig. 13e). The Kufrah River paleowatershed, at its maximum extent, would represent close to a quarter of the surface area of Libya. Our gravitational results suggest that both paths in Fig. 13e are possible.

We envisage space for paleorivers and paleolakes in NW Egypt, beneath the present-day part of the Grand Sand Sea (Fig. 14a–d). Clearly marked are a negative band of T_{zz} (Fig. 14a) and of the depression (vd in Fig. 14b) and the extremes in I_2 (in Fig. 14c). A flow logically comes out from south to north along the present-day border between Egypt and Libya, all in accord with the topography (Fig. 14d)—there is a slope from S to N to the Siwa and Qattara depressions nearby. We speculate about the outflow in W and NW directions to Libya and then to the Mediterranean Sea (gravitational signal permits few alternatives). The reader can watch it mainly in Fig. 14b–d (and with previous series of Fig. 13a–f). A

possible connection of this area with the parts of West Egypt north of Uweinat and Arkenu mountains and Gilf Kebir (Great Barrier) for $\varphi = 22\text{--}29^\circ$ is shown in Fig. 14e, f: (e) is for I_2 and (f) for vd .

The Nile, Wadi Tushka and possible Kharga paleomegalake

There are more chances for the existence of paleolakes and paleorivers on the territory of present-day Egypt (and partly Sudan, Fig. 15a), not only the cases shown by Fig. 14a–f.

Note strong negative T_{zz} (Fig. 15a), connected with the middle and lower reaches of the Nile River, with its deep and wide valleys; Faiyum (al-Fayyūm) oasis ($\varphi = 29\text{--}30^\circ$ N, $\lambda = 30\text{--}31^\circ$ E); delta of the Nile, Grand Sand Sea/Western Desert and Siwa and Qattara depression ($27\text{--}30^\circ$, $25\text{--}28^\circ$); oases Dakhla, Farafra and Baharia ($25\text{--}27^\circ$, $27\text{--}29^\circ$); Wadi Toshka or Tushka ($22\text{--}23^\circ$, $31\text{--}32^\circ$), related via relicts of (Toshka) Lakes ($22\text{--}23^\circ$, $30\text{--}31^\circ$) to N to the valley and town Kharga/Charga (with possible northern end of the megalake, $23\text{--}26^\circ$, $30\text{--}31^\circ$). Analogically, a strong signal can be found by the invariants and vd (not shown here).

A comparison with topography focused on the case of southern Egypt and adjacent Sudan (Fig. 15b, c) and details of the gravitational signal in this area follow in Fig. 15e, f. First, we show the topography from the SRTM DEM (in Fig. 15b, from Maxwell et al. 2010) with overflow of Nile River to W through Wadi Toshka (height difference ~ 20 m) and then topography from the ASTER GDEM (in Fig. 15c). Water may flow through Wadi Tushka via lakes remnants in the W direction into a hypothetical paleomegalake, reaching on its northern end Kharga. Its length from south to north might be 350 km and its depth about 100 m. Then it might continue to NE or NW. The gravitational signal in Fig. 15a, f illustrates a possible configuration of the paleoriver and megalake. Our results support those in Maxwell et al. (2010).

Landsat and Radarsat images unveiled evidence of an ancient megalake in Darfur (northwestern Sudan). The size of the lake should be about 200×200 km. We were not successful to support these results by our gravitational data; the “signal” is not significant enough.

We did not investigate other possible paleolakes and paleorivers in Africa outside the Sahara (such as the hypothetical megalake Congo or a megalake on the Nile in Sudan, e.g. Williams et al. 2010; Whiteman 1971), because this search would be complicated by other local geological phenomena. Some areas, however, can be tested on request (contact please the first author), but one has carefully accounted for nearby geological structures, for resolution of our method, non-uniqueness of the gravitational signal, possible disturbing artefacts or presence of the fill-in data in all recent combined gravitational field models.

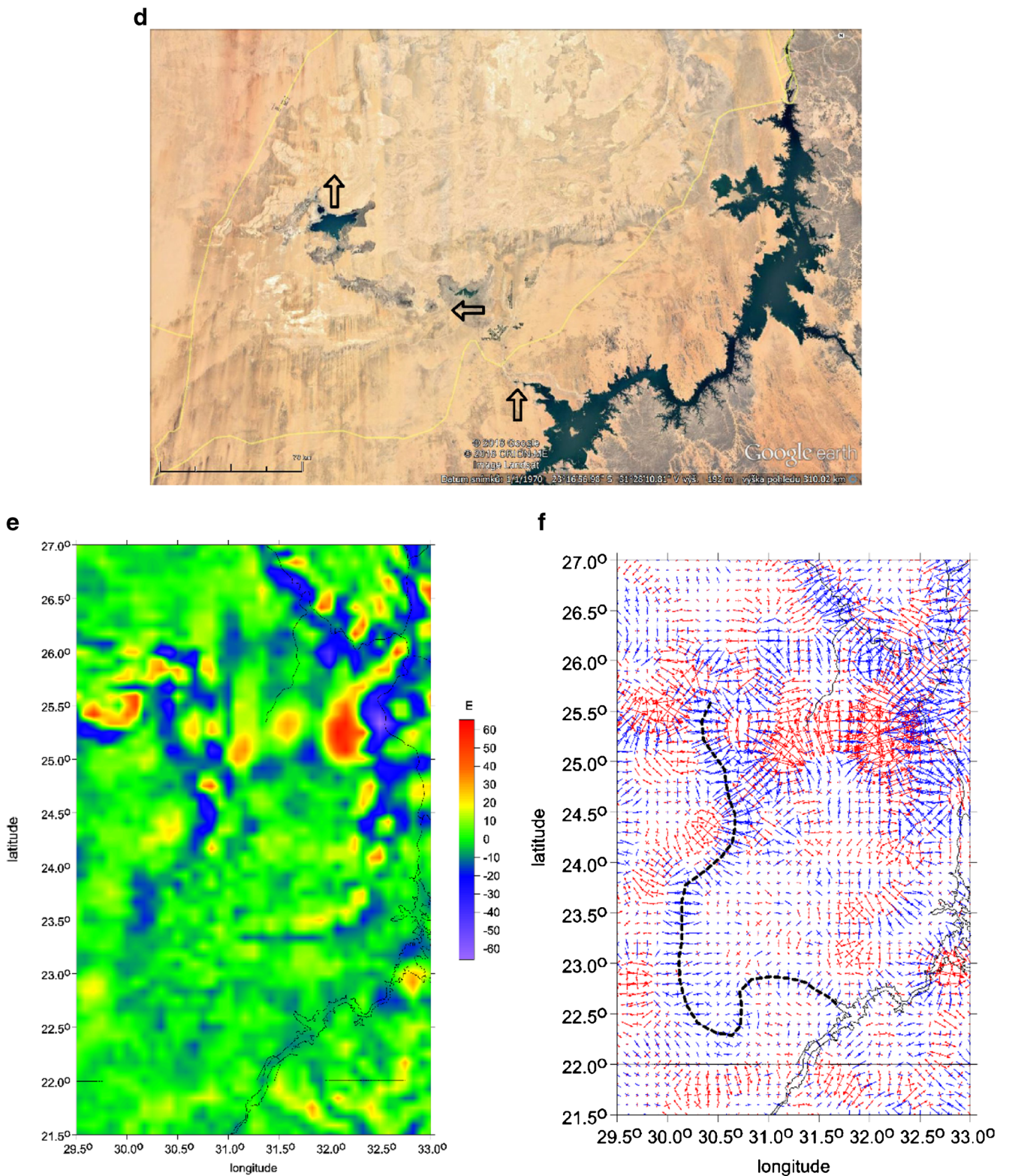


Fig. 15 continued.

Concluding remarks

It is always important to have independent analyses supporting certain results achieved by other researches, and

this paper is such a case. We demonstrated that and how the recent gravitational and topographic data support findings made by geologists and others as for the existence of paleolakes and paleoriver systems, now buried under the

sands of Sahara. Various functions of the disturbing gravitational potential (the aspects) were computed and plotted for the whole planet Earth, in step 5×5 arcmin with the global gravitational model EIGEN 6C4 and with two global topography models ASTER GDEM and ETOPO 1. Many examples have already been presented elsewhere [e.g. Kalvoda et al. (2013), Klokočník et al. (2010, 2013, 2016)]. Here we focused on the specific areas of the Sahara, where geologists found paleolakes and rivers now mostly or completely parched and covered by sand. We tested how the gravitational signal contributes to a confirmation (and perhaps also to an extension) of their discoveries and we nearly always supported the conclusions of geologists).

It was necessary to critically review our input data, namely as for the areas with the fill-in (topographic) data used in the gravity field model EIGEN 6C4, as for a resolution of this model on the ground or various artefacts created usually due to a low quality of the local terrestrial data and due to their gridding. We show that the signal to noise ratio (a difference between the gravity anomaly inside and closely outside the hypothetical paleolake divided by an accuracy estimate of the gravity anomalies in EIGEN 6C4) is sufficiently large (>3) to be statistically significant.

We work not only with the gravity disturbances/anomalies but also with the full Marussi tensor of the second derivatives of the disturbing potential, with the gravity invariants, their specific ratio, with the strike angle and virtual deformations (for theory, see Pedersen and Rasmussen 1990; Beiki and Pedersen 2010; Kalvoda et al. 2013; Klokočník et al. 2010, 2013, 2016). To learn how the typical gravitational signal from all these functions (aspects) of the geopotential looks like for various geological objects (volcanoes, faults, impact craters...), we provided various examples in the section “Typical gravitational signal of various geological structures, note on artefacts” (and much more examples can be found in our already quoted papers).

We modelled megalakes filled by sand (instead of water) as for their gravity anomalies and the second radial derivative for the various shapes of lakes and their depth, and tested how large gravitational signal can be expected from a megalake with various thickness of the sand layer. We found that our model can explain what is observed in reality, meaning that in majority of the studied cases, the observed “gravity” comes dominantly from a paleolake.

Our choice of the Saharan areas was focused on places relatively “gravitationally silent”, undisturbed by big mountain belts, fracture zones, etc. All selected segments have now “flat” topography (“sand and dune seas”) but often not “flat” gravitational signal. We studied localities of the paleolakes MegaChad, Fazzan and Chotts; the area related to a paleoriver system Tamanrasset; and in east Libya, northwest Egypt (Grand Sand Sea) or south Egypt (from Wadi Toshka to Kharga). Our results are presented in

the section “Gravitational signal and topography for selected zones of Sahara with EIGEN 6C4 and ASTER GDEM”; with them, we support the conclusions from Leblanc et al. (2006) and Armitage et al. (2015) for the paleolake MegaChad, from Drake et al. (2008) for MegaFazzan, for MegaChotts from Skonieczny et al. (2015), for Tamanrasset from Drake et al. (2008) or Paillou et al. (2012) for east Libya (including Kufrah Basin) or from Maxwell et al. (2010) for the area between Wadi Tushka/Kharga. Moreover, we suggest the existence of a paleolake and rivers in northwestern Egypt roughly beneath the Great Sand Sea, flowing from south to today’s oasis Siwa and nearby depression and in the west direction to Libya with intake to the Mediterranean (Fig. 14a–f).

Our findings suggest a completely different view of the Sahara region. Relicts of small lakes are well known in numerous places of Egypt, Libya and other countries (Embabi 2004), but the existence of several megalakes points more to the landscape resembling contemporary Lake Victoria in eastern Africa.

The intensive gravitational anomalies such as south of Siwa in Egypt display the widespread existence of large and deepening lake basins that must be in the majority of cases older than Quaternary and possibly Miocene (approx. >20 Ma) in origin (Said 1990, 1993). The belt of oases in Egyptian Western Desert is probably established on the relicts of the former Nile valley, that was during Oligocene-Upper Miocene (34–5 Ma) dissected and partially uplifted by Neoid movements. Intensive aeolian planation then took place in dry phases of Quaternary (2.7 Ma to present), but some parts of the former valley were later exhumed by strong winds during glacials. Therefore, we tend to look at Saharan landscapes as characteristic African etchplain on which (during humid phases) very large but shallow—in some cases probably intermittent—lakes existed, encircled by riverine systems. While the ground penetrating radar discovers numerous but mostly shallow wadis—so-called radar rivers—the changes of gravitational field indicate relicts of valleys of comparable size as present-day Nile (McHugh et al. 1988).

These lake basins later probably several times dried up; their segments were uplifted or submerged by Neoid tectonics (Issawi and Al-Miṣrīyah 1999), but the lower tectonic escarpments and ridges unlike in eastern and southern Africa were destroyed by wind abrasion resulting in a new phase of planation. Therefore, we propose not only the existence of large Cenozoic lakes but different morphological histories of the Saharan region as well (Burke and Gunnell 2008).

One of the authors twice crossed the Egyptian Western Desert during archaeological expeditions aimed at the understanding of the old roads from the Old Kingdom and in Silica region. Large lake basins like Silica are virtually invisible on the present desert surface due to long-lasting

wind abrasion and thanks to a cover by younger aeolian sediments which were often removed by scarce torrential rains and then again covered by reblown sand.

We are thus aware that our mostly hypothetical findings established on analogy with proven or existing lake basins such as Faiyum (flooded in some cases by shallow Miocene seas, Dumont 2009) must be verified by field drilling research, but we need to point out that the satellite gravitational data (now from GOCE) are opening new insights and indications of major Saharan lost rivers and paleolakes (and much more).

Our method works and can in the future be strengthened by new gravitational models and other data—it means more reliable (less fill-in areas in the gravity models) and more accurate data and with data having better resolution. Further localities can be tested on request but not always and not everywhere a success can be guaranteed. Geological data and our results indicate locations where further paleontological, paleoanthropological and archaeological field explorations should be conducted.

Acknowledgements This work has been prepared in the frame of projects #13-36843S (Grant Agency of the Czech Republic) and RVO #679 858 15 (Czech Academy of Sciences), partly supported by the project LO 1506 (PUNTIS) from Ministry of Education of the Czech Republic. We are obliged to Ing. B. Bucha, PhD (STU Bratislava) for computations of the functions of the disturbing potential (here EIGEN 6C4) and Ing. Karolina Hanzalová for a part of topographic data.

Appendix - artefacts

We recall sections “Gravitational field models with high resolution”, “Typical gravitational signal of various geological structures, note on artefacts” and “Lake MegaFazzan”. The method of solution for the harmonic geopotential coefficients is in fact a type of Fourier analysis. The input data are inevitably gridded (they are not continuous), and thus, the mathematical process generates “false” harmonic frequencies. As an example, let us take the function “sinus” defined on the interval $\langle 0^\circ, 360^\circ \rangle$ by the individual data points given in an interval 20° (Fig. 16). After the Fourier transform, we receive a frequency spectrum shown in Fig. 17. Due to the gridding, we observe many frequencies and not the expected “theoretical” period of 360° . The most important frequencies, together with their amplitudes, are gathered into Table 2. By this way, we explain at least some of the artefacts discussed in sections “Typical gravitational signal of various geological structures, note on artefacts” and “Gravitational signal and topography for selected zones of Sahara with EIGEN 6C4 and ASTER GDEM”. Besides this, we can observe classical big “long-wave” aliasing effect (Fig. 18), originating when very few observations would be available in the interval $\langle 0^\circ, 360^\circ \rangle$. The artefacts depend on the density of the input data and on numerical precision of the transform.

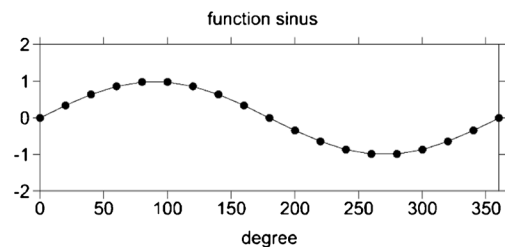


Fig. 16 The input data to Fourier analysis; data interval is 20°

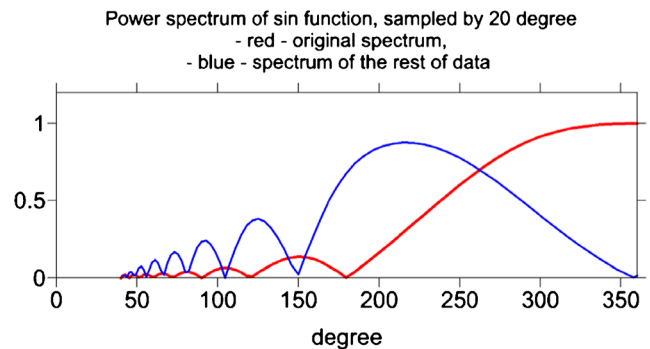


Fig. 17 Output from the Fourier transform; the frequency spectrum with artefacts

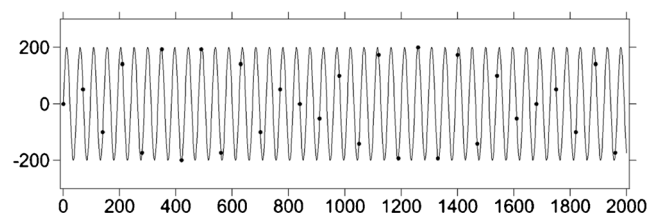


Fig. 18 The well-known aliasing as a “long-wave” artefact. The long wave would constitute from the dots

Table 2 The approximation of the function “sinus” on the interval $\langle 0^\circ, 360^\circ \rangle$. The most important frequencies, together with their amplitudes, after the Fourier transform of “sinus” function with the gridded input data

Period [°]	Amplitude
360	1.0077
215	0.0131
150	0.0050

References

- Amante C, Eakins BW (2009) ETOPO1, 1 arc-minute global relief model: procedures, data sources and analysis. NOAA Techn. Memo. NESDIS NGDC-24. National Geophysical Data Center, NOAA. doi:10.7289/V5C8276M

- Andrews-Hanna JC, Sami W, Asmar JW et al (2012) Ancient igneous intrusions and early expansion of the moon revealed by GRAIL gravity gradiometry. *Science Express*. doi:10.1126/science.1231753
- Armitage SJ, Bristol CS, Drake NA (2015) West African monsoon dynamics inferred from abrupt fluctuations of Lake Mega-Chad. *Proc National Acad Sci* 112(28):8543–8548
- Battarbee R, Gasse F, Stickley C (2004) Past climate variability through Europe and Africa. Springer, Dordrecht 420 pp
- Beiki M, Pedersen LB (2010) Eigenvector analysis of gravity gradient tensor to locate geologic bodies. *Geophysics* 75:137–149. doi:10.1190/1.3484098
- Braitenberg C, Mariani P, Ebbing J, Sprlak M (2011) The enigmatic Chad lineament revisited with global gravity and gravity-gradient fields. In: Van Hinsbergen et al. (eds) *The formation and evolution of Africa: a synopsis of 3.8 Ga of Earth history*. *Geol Soc Lond Spec Publ*, 357: 329–341. doi: 10.1144/SP357.18 0305-8719/11
- Brdička M, Samek L, Sopko B (2000) *Mechanika kontinua (continuum mechanics)*. Academia Publ. House, Praha (in Czech)
- Bucha B, Janák J (2013) A MATLAB-based graphical user interface program for computing functionals of the geopotential up to ultra-high degrees and orders. *Comput Geosci* 56:186–196. doi:10.1016/j.cageo.2013.03.012
- Burke K, Gunnell Y (2008) The African erosion surface: a continental-scale synthesis of geomorphology, tectonics, and environmental change over the past 180 million years. *Memoir* 201:37–44 Boulder, Colorado
- Dietz RS, Fudali R, Cassidy W (1969) Richat and Semsiyat domes (Mauritania): not Astroblemes. *Geological Society of America* 80(7):1367–1372
- Drake NA, El-Hawat AS, Turner P, Armitage SJ, Salem MJ, White KH, McLaren S (2008) Palaeohydrology of the Fazzan Basin and surrounding regions: the last 7 million years. *Palaeogeogr Palaeoclimatol Palaeoecol* 263:131–145
- Dumont HJ (ed) (2009) *The Nile. Origin, environments, limnology and human use*. Springer, Berlin, pp 52–120
- Embabi NS (2004) *The geomorphology of Egypt. Landform evolution. Vol. I, the Nile Valley and the Western Desert*. The Egyptian Geographical Society, Cairo, pp 32–70
- Foerste Ch, Bruinsma S, Abyrkosov O, Lemoine J-M et al (2014) The latest combined global gravity field model including GOCE data up to degree and order 2190 of GFZ Potsdam and GRGS Toulouse (EIGEN 6C4). 5th GOCE user workshop, Paris 25–28, Nov. 2014
- Hoelzmann P, Gasse F, Dupont LM et al (2004). In: Battarbee et al. (eds.) *Paleoenvironmental changes in the arid and subarid belt (Sahara-Sahel-Arabian peninsula) from 150 kyr to present*, pp. 219–256
- Holmes SA, Pavlis NK, Novák P (2006) A Fortran program for very-high degree harmonic synthesis, version 05/01/2006
- Hotine M (1969) *Mathematical Geodesy*, ESSA, US. Dept. Comm., Environ. Sci. Serv. Admin., Monograph 2, Washington D.C.
- Huang J, Reguzzoni M, Gruber T, eds. (2015) *Assessment of GOCE geopotential models*, Newton's Bull. 5. IAG & IGFS. ISSN 1810-8555
- Issawi B, Al-Miṣrīyah MJ (1999) *The Phanerozoic geology of Egypt. A geodynamic approach*. The Egyptian Geologic Survey, Cairo 462 pp
- Jesus MF, Fernando RP, Paz MRM et al (2011) Multianalytical characterization of silica-rich megabreccias from the proposed natural area of Richat (Sahara desert, Mauritania). *Res J Chem Environ* 15(3)
- Kafri U, Yechieli Y (2010) Groundwater base level changes and adjoining hydrological systems, Sect. 11.6. Springer. ISBN 978-3-642-13943-7
- Kalvoda J, Klokočník J, Kostelecký J, Bezděk A (2013) Mass distribution of Earth landforms determined by aspects of the geopotential as computed from the global gravity field model EGM 2008. *Acta Univ. Carolinae, Geographica*, XLVIII, 2, Prague, Czech Rep
- Klokočník J, Kostelecký J, Pešek I, Novák P, Wagner CA, Sebera J (2010) Candidates for multiple impact craters? Popigai and Chicxulub as seen by the global high resolution gravitational field model EGM08. *Solid Earth EGU* 1:71–83. doi:10.5194/se-1-71-2010
- Klokočník J, Kalvoda J, Kostelecký J, Eppelbaum L, Bezděk A (2013) Gravity disturbances, Marussi tensor, invariants and other functions of the geopotential represented by EGM 2008, presented at ESA Living Planet Symp. 9–13 Sept. 2013, Edinburgh, Scotland; publ. in Aug. 2014 in. *JESR (J Earth Sci Res)* 2: 88–101
- Klokočník J, Kostelecký J, Pešek I, Bezděk A (2016) On feasibility to detect volcanoes hidden under the ice of Antarctica via their “gravitational signal”. *Ann Geophys* 59. doi:10.4401/ag-7102
- Kuper R, Kröepelin S (2006) Climate-controlled Holocene occupation in the Sahara: motor of Africa's evolution. *Science* 313:803–807
- Leblanc M, Favreau G, Maley J et al (2006) Reconstruction of Megalake Chad using Shuttle radar topographic mission data. *Palaeogeogr Palaeoclimatol Palaeoecol* 239:16–27
- Lopez T, Antoine R, Kerr Y, Darrozes J, Rabinowicz M, Ramillien G, Cazenave A, Genthon P (2016) Subsurface hydrology of the Lake Chad basin from convection modelling and observations. *Surv Geophys* 37:471–502. doi:10.1007/s10712-016-9363-5
- Marty JC, Balmino G, Duron J, Rosenblatt P et al (2009) Martian gravity field model and its time variations from MGS and Odyssey data 2009. *Planetary and Space Science* 57(3):350–363. doi:10.1016/j.pss.2009.01.004
- Mataragio J, Kieley J (2009) Application of full tensor gradient invariants in detection of intrusion-hosted sulphide mineralization: implications for deposition mechanisms. *Mining Geoscience, EAGE First Break*, 27: 95–98
- Matton G, Jébrak M (2014) The “eye of Africa” (Richat dome, Mauritania): an isolated cretaceous alkaline–hydrothermal complex. *J Afr Earth Sci* 97(8):109–124
- Maxwell TA, Bahay Issawi, Vance Haynes Jr. C (2010) Evidence for pleistocene lakes in the Tushka region, south Egypt. Downloaded from geology.gsapubs.org on November 22
- McHugh W, McCauley JF, Haynes V, Breed CS, Schaber GG (1988) Paleorivers and geoarchaeology in the Southern Egyptian Sahara. *Geoarchaeology* 3(1):1–40
- Murphy CA, Dickinson JL (2009) Exploring exploration play models with FTG gravity data. 11th SAGA Biennial Techn. Meeting & Exhib., Swaziland, pp 89–91
- Paillou P, Tooth S, Lopez S (2012) The Kufrah paleodrainage system in Libya: a past connection to the Mediterranean Sea? *Compt Rendus Geosci* 344(8):406–414. doi:10.1016/j.crte.2012.07.002
- Pajot G, Diament M, Lequentrec-Lalancette M-F, Tiberi Ch (2004) A Bayesian approach to invert GOCE gravity gradients. *Proc. 2nd Internatl. GOCE User Workshop ESA-ESRIN, Frascati, ESA SP-569*
- Patriat M, Ellouz N, Dey Z, Jean-Michel Gaulie J-M, Ben Kilani H (2003) The Hammamet, Gabés and Chotts basins (Tunisia): a review of the subsidence history. *Sediment Geol* 156:241–262
- Pavlis NK, Holmes SA, Kenyon SC, Factor JK (2008a) An Earth gravitational model to degree 2160: EGM 2008. *EGU General Assembly 2008, Vienna*
- Pavlis NK, Holmes SA, Kenyon SC, Factor JK (2008b) EGM2008: an overview of its development and evaluation. National Geospatial-Intelligence Agency, USA, conf.: Gravity, Geoid and Earth Observation 2008, Chania, Crete, Greece
- Pavlis NK, Holmes SA, Kenyon SC, Factor JK (2012) The development and evaluation of the Earth gravitational model 2008 (EGM2008). *J Geophys Res* 17:B04406. doi:10.1029/2011JB008916
- Pedersen BD, Rasmussen TM (1990) The gradient tensor of potential field anomalies: some implications on data collection and data processing of maps. *Geophysics* 55:1558–1566
- Saad AH (2006) Understanding gravity gradients—a tutorial, the meter reader. In: Van Nieuwenhuise B, August issue, *The Leading Edge*, 941–949
- Said R (1990) *The geology of Egypt*. A.A. Balkema, Rotterdam 720 pp.

- Said R (1993) The river Nile. Geology, hydrology and utilization. Pergamon, Oxford, 320 pp
- Salem MJ, Busrewil MT (1980) The geology of Libya. I–III, 1200 pp. Academic, London.
- Schlütter T (2006) Geological atlas of Africa: 218–220. Springer, Berlin
- Schuster M, Roquin C, Durringer P, Brunet M, Fontugne M, Mackaye HT, Vignaud P, Ghienne J-F (2005) Holocene Lake Mega-Chad palaeo-shorelines from space. *Quat Sci Rev* 24(16–17):1821–1827
- Sebera J, Wagner CA, Bezděk A, Klokočník J (2013) Short guide to direct gravitational field modelling with Hotine's equations. *J Geod* 87:223–238. doi:[10.1007/s00190-012-0591-2](https://doi.org/10.1007/s00190-012-0591-2)
- Skonieczny C, Paillou P, Bory A, Bayon G, et al (2015) African humid periods triggered the reactivation of a large river system in Western Sahara. *Nat Commun* 6, Article number: 8751. doi:[10.1038/ncomms9751](https://doi.org/10.1038/ncomms9751)
- Whiteman AJ (1971) The geology of the Sudan Republic. Clarendon, Oxford, pp 52–64
- Williams MAJ, Williams FM, Dulle GAT et al (2010) Late Quaternary floods and droughts in the Nile Valley, Sudan: new evidence from optically stimulated luminescence and AMS radiocarbon dating. *Quat Sci Rev* 29:1116–1137